CHALMERS
UNIVERSITY OF TECHNOLOGY

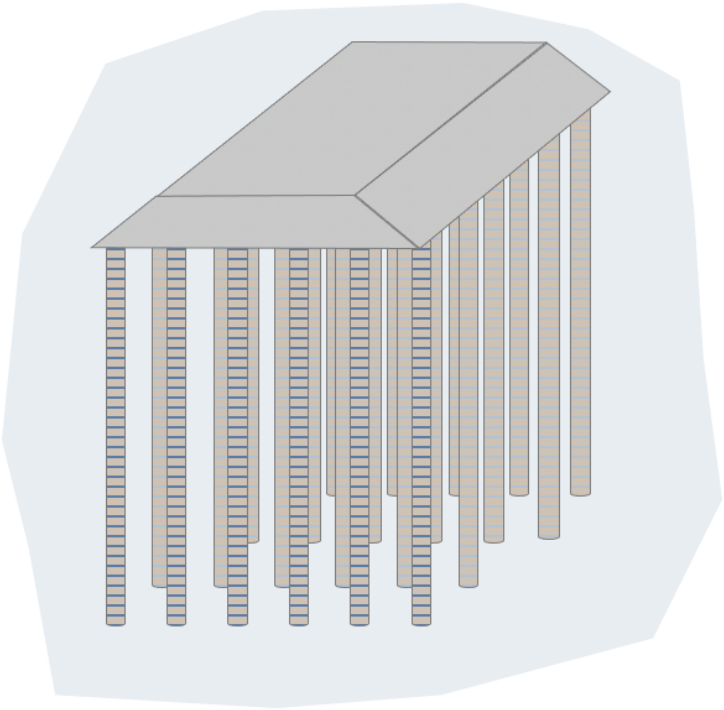

Effects of Lime-Cement Column Characteristics on the Performance of an Embankment on Soft Clay

An Analysis Using Volume Averaging Technique in Plaxis 2D

Master's Thesis in Infrastructure and Environmental Engineering

ELIN HÖJER
KRISTIN OLOFSSON HOFFMANN

DEPARTMENT OF ARCHITECTURE AND CIVIL ENGINEERING
DIVISION OF GEOLOGY AND GEOTECHNICS

CHALMERS UNIVERSITY OF TECHNOLOGY
Gothenburg, Sweden 2022
www.chalmers.se

Master's thesis 2022

Effects of Lime-Cement Column Characteristics on the Performance of an Embankment on Soft Clay

An Analysis Using Volume Averaging Technique in Plaxis 2D

Elin Höjer
Kristin Olofsson Hoffmann

CHALMERS
UNIVERSITY OF TECHNOLOGY

Department of Architecture and Civil Engineering
Division of Geology and Geotechnics
Chalmers University of Technology
Gothenburg, Sweden 2022

Effects of Lime-Cement Column Characteristics on the Performance of an Embankment on Soft Clay
An Analysis Using Volume Averaging Technique in Plaxis 2D
Elin Höjer
Kristin Olofsson Hoffmann

Supervisor: Ayman Abed, Department of Architecture and Civil Engineering
Examiner: Minna Karstunen, Department of Architecture and Civil Engineering

Master's Thesis 2022
Department of Architecture and Civil Engineering
Division of Geology and Geotechnics
Chalmers University of Technology
SE-412 96 Gothenburg
Telephone +46 31 772 1000

Cover: Embankment on lime-cement columns.

Typeset in LaTeX
Printed by Chalmers Reproservice
Gothenburg, Sweden 2022

Effects of Lime-Cement Column Characteristics on the Performance of an Embankment on Soft Clay
An Analysis Using Volume Averaging Technique in Plaxis 2D
ELIN HÖJER
KRISTIN OLOFSSON HOFFMANN
Department of Architecture and Civil Engineering
Chalmers University of Technology

Abstract

Lime-cement columns are commonly used in Sweden as a ground improvement method. In this thesis a system consisting of an embankment on lime-cement columns is studied. The aim of the study is to investigate the impact of lime-cement column characteristics on the stress-strain response of the described system. It is also investigated how well the use of column guideline values from Trafikverket complies with the stress strain response of lime-cement columns measured in field. The embankment, located in Nödinge north of Gothenburg, is a former full-scale test embankment part of a feasibility study for the development of a new motorway and high-speed railway. When modelling lime-cement columns under an embankment a full 3D analysis is needed, something which is both time consuming and complicated to conduct. Thus, in this thesis the system was modelled using the Volume Averaging Technique (VAT) in Plaxis 2D. The VAT-model implements two constitutive models, S-CLAY1S and MNhard, for the soil and the columns, respectively, and converts the 3D problem to a 2D problem.

The study shows that an increased column stiffness leads to decreased settlements. However, the effect of the column stiffness on the deformation behaviour seems to lessen with increasing column stiffness. Furthermore, the predicted vertical displacements using a column stiffness corresponding to Trafikverket's guideline values are significantly larger than those measured at the site. This indicates that the stiffness of the columns in Nödinge is much higher than the stiffness given by the guideline values. The results are further supported by laboratory tests on lime-cement column samples which also showed higher stiffnesses than the guidelines. However, the laboratory tests also exhibit a large span of stiffnesses. This suggests that it is necessary to have lower guidelines to account for the uncertainties regarding the column stiffness. Since cement is a large contributor to the world's CO_2-emissions, it is of great interest to lower the amount of stabiliser used. Therefore, further investigations on how well the guidelines coincides with the actual stiffness of lime-cement columns used in field, are suggested.

Keywords: Embankment, Lime-Cement Columns, S-CLAY1S, MNhard, Volume Averaging Technique, Settlements, Plaxis 2D

Acknowledgements

First and foremost, we would like to thank our supervisor and examiner Minna Karstunen, professor at Chalmers University of Technology for introducing us to the subject and providing us with valuable guidance and support. Just as valuable was the help and guidance from our supervisor Ayman Abed, senior lecturer at Chalmers University of Technology. The conducted modelling in Plaxis 2D using VAT would not have been possible without his help.

We would also like to express our gratitude towards Sinem Bozkurt at Chalmers University of Technology for her guidance and for supplying us with data for the lime-cement columns. Furthermore, we would like to thank Mats Karlsson at Chalmers University of Technology for giving us knowledge and necessary data from the Nödinge test site.

Finally, we would like to thank all of them for their patience with our countless questions. Without them this thesis would not have been possible.

Elin Höjer & Kristin Olofsson Hoffmann, Gothenburg, June 2022

List of Acronyms

Below is the list of acronyms that have been used throughout this thesis listed in alphabetical order:

CSL	Critical State Line
DSM	Deep Soil Mixing
HS	Hardening Soil
MN	Matsuoka-Nakai
VAT	Volume Averaging Technique
UDSM	User Defined Soil Model

Nomenclature

Below is the nomenclature that have been used throughout this thesis.

Indices

c	Index for columns
s	Index for soil
eq	Index for homogenised material

Roman Letters

a	Absolute rate of destructuration
b	Relative effectiveness of destructuration
c	Cohesion
c'	Effective cohesion
c_{crit}	Critical shear stress
e	Void ratio
e_0	Initial void ratio
f_t	Allowable tensile stress
k	Hydraulic conductivity
m	Power of hyperbolic stress-strain law
p'	Mean effective stress
p'_m	Size of the yield surface
p'_{mi}	Size of the intrinsic yield surface
p'_{ref}	Reference pressure for hyperbolic stress-strain law
q	Deviator stress
q_f	Deviatoric stress at failure
x	Amount of bonding
x_0	Initial amount of bonding

Roman Capital Letters

$\boldsymbol{D}$	Stiffness matrix
E	Young's modulus
E'	Effective Young's modulus
E_{oed}	Oedometer modulus
E_{ur}	Unloading/reloading modulus
E_{50}	Secant stiffness modulus
E'_{50}	Effective secant stiffness moduls
E_{50}^{ref}	Reference stiffness modulus at reference stress
G	Shear modulus
G'_{50}	Effective secant shear modulus
G_{ur}^{ref}	Reference shear modulus for unloading/reloading
G_{50}^{ref}	Reference shear modulus for primary loading
K_0	Coefficient of earth pressure at rest
M_c	Critical state stress ratio
OCR	Over consolidation ratio
POP	Pre overburden pressure
R_f	Failure ratio
$\boldsymbol{S_1}$	Relation of strain increments
$Skempton - B$	Skempton-B for undrained loading

Greek Letters

α	Scalar inclination of the yield surface
α_0	Initial inclination of the yield surface
β	Shear and volumetric strain's effectiveness in rotating the yield surface
$\dot{\gamma}$	Shear strain in axial direction
γ_s^{ps}	Objective shear strain
γ_{unsat}	Unsaturated unit weight
γ_{sat}	Saturated unit weight
ε_1	Major principal strain
ε_2	Intermediate principal strain
ε_3	Minor principal strain

$\dot{\boldsymbol{\varepsilon}}$	Strain tensor
$\dot{\varepsilon}$	Strain in axial direction
ε^p	Plastic strain
ε_d^p	Plastic shear strain
ε_v^p	Plastic volumetric strain
η	Stress ratio
η_0	Stress state at the normally consolidated state
θ	Lode angle
κ	Swelling index
λ	Compression index
λ_i	Intrinsic compression index
μ	Absolute rate of change of the yield surface inclination
ν	Poisson's ratio
ν'	Poisson's ratio for drained conditions
ρ	Density
σ_1	Major principal stress
σ_2	Intermediate principal stress
σ_3	Minor principal stress
σ'_1	Major principal effective stress
σ'_2	Intermediate principal effective stress
σ'_3	Minor principal effective stress
σ'_c	Preconsolidation pressure
σ'_V	Effective vertical stress
$\dot{\boldsymbol{\sigma}}$	Stress tensor
$\dot{\sigma}$	Stress in radial direction
σ_t	Tension cut-off and tensile strength
$\dot{\tau}_{xy}^c$	Shear stress in radial direction
ϕ	Friction angle
ϕ'	Effective friction angle
ϕ'_m	Mobilised friction angle
ψ	Dilatancy angle
ψ'	Effecitve dilatancy angle
Ω_c	Volume ratio

Contents

List of Figures

List of Tables

1
Introduction

1.1 Background

Soft soils such as soft clays are often improved with lime-cement columns, a type of deep soil mixing (DSM) where cement and lime are mixed into the soil in situ. These improvements are performed to reduce settlements and increase the stability of the soil. The deep mixing is commonly used in Sweden and has been since its introduction in 1970 (Larsson, 2006). To ensure safe usage of the technique in Sweden, the Swedish Transport Administration (Trafikverket) has developed a set of guidelines for the design (Karlsson & Moritz, 2014). These are presented in two reports, TK Geo (Karlsson & Moritz, 2014) and TR Geo (Moritz & Karlsson, 2016), containing technical requirements and recommendations associated to the requirements.

When modelling lime-cement columns under an embankment a full 3D analysis is needed, something which is both time consuming and complicated to conduct. Recently, a model converting the 3D modelling into 2D has been developed at Chalmers University of Technology, based on prior PhD work at the University of Wales Swansea and the University of Strathclyde. The method is called Volume Averaging Technique (VAT) and it has been proven to give results similar to those of 3D analyses. When using the VAT method the two individual constituents, soil and column, are modelled as a composite material, yet tracking the emerging stiffness and strength of the constituents, thus simplifying the three-dimensional problem into a two-dimensional problem (Vogler, 2008).

In the Göta River valley, located in the west of Sweden, the majority of the soil consists of soft clay. The characteristics of the soil and stratigraphy originate from the deposition history in the area and are a result of the latest ice age which occurred around 110 000 - 6 000 BC (Statens Geotekniska Institut, 2009). During this period, Sweden was covered by a 2-4 km thick layer of ice, pressing down the bedrock. As a consequence, the Göta river valley was submerged in the sea for thousands of years following the ice melting, during which clay was deposited at the sea bottom. Due to post-glacial rebound, the land surface was successively lifted above sea level again and as a result several areas along the Göta river consist of previous marine soil layers with a stratigraphy that contains thick layers of soft clay.

As can be seen in Figure 1.1, the urban area of Nödinge is located next to the Göta River. A full-scale test embankment was constructed there in 2001 to study the per-

formance of floating lime-cement columns for settlement reduction (Olsson, 2010). The embankment was constructed as part of a feasibility study for the development of a new motorway and high-speed railway between Gothenburg and Trollhättan. Further research has been carried out at the site, and therefore extensive measurement data of settlements and pore pressures are available. Data regarding the characteristics of the lime-cement columns are however restricted. Since the test embankment was removed in 2007, no new data is available.

Figure 1.1: Map showing the location of Gothenburg and Nödinge along the Göta River. Modified map from Google (2022).

1.2 Aim

This thesis aims to investigate the impact of lime-cement column characteristics on the stress-strain response of a system consisting of an embankment on lime-cement column reinforced soil. This will be done using the Volume Averaging Technique in Plaxis 2D to model the test embankment in Nödinge. The following questions will additionally be answered:

- How do the modelled settlements compare to those measured at the site in Nödinge?
- How well do the column guidelines from Trafikverket correspond with the modelled and measured deformation behaviour of the lime-cement reinforced system in Nödinge?

1.3 Limitations

The thesis have several limitations, these are listed below. Furthermore, the work is affected by the limitations of each used constitutive model, these are described further in Chapter 2.

- There is limited knowledge on the locations of the boreholes at the Nödinge test site.
- There is a lack of data regarding the characteristics of the installed lime-cement columns at the Nödinge Test embankment.
- The destructuration behaviour of the soil is not considered.
- Creep effects are not included in the Volume Averaging Technique.
- The effect of the lime-cement column characteristics on the stability of the embankment will not be considered.
- The stiffness is the only column characteristics considered when investigating the impact on the stress-strain response.

1.4 Method Overview

Overall, the methodology was divided into three main steps; literature study, derivation of input data and numerical modelling in Plaxis 2D. A literature study was performed to gather information on lime-cement columns in general, as well as the constitutive models used to describe the natural and reinforced soil in Plaxis 2D. The soil and column data were derived partly from literature and partly from data from field and laboratory tests. The literature sources consisted mainly of reports connected to the feasibility study and further research of the full-scale test embankment in Nödinge. The soil test facility in Plaxis 2D was used to confirm and modify the laboratory test result. Lastly, the lime-cement reinforced system in Nödinge was modelled in Plaxis 2D using the Volume Averaging Technique. The S-CLAY1S model and the MNhard model was used to model the two constituents, soil and column, respectively.

2
Theory

2.1 Lime-Cement Columns

Lime-cement columns are used as a form of stabilisation of soil (Carlsten, 2000). Lime and cement are mixed with the soil in situ, creating columns which improves the stability and reduces settlements (Vogler & Karstunen, 2009). The columns have been proven efficient in very soft clay, organic soils and silts. The mixture of lime and cement is the most common binder material for soil stabilisation used in Sweden, although binder materials consisting of only lime or cement are used as well (Larsson, 2006).

Due to the lime-cement columns' abilities to decrease settlements and increase characteristics such as shear strength, compression modulus and rate of consolidation (Carlsten, 1996), it has become a widely used reinforcement method. To some extent, lime-cement columns can replace embankment piles and vertical drains (Larsson, 2006). In Sweden lime-cement columns are mainly used as reinforcement of soft soil beneath road and railway embankments and small bridges. The technique can further be used to stabilise excavated and natural slopes, as well as to reduce earth pressure against sheet pile walls (Carlsten, 1996). However, for stabilisation of natural slopes it is normally not used, as the only measure and precautions such as monitoring of pore pressures and soil movements must be taken to ensure the stability of the slope (Larsson, 2006).

The columns are created by mixing a binder (e.g. lime or lime-cement) with the natural soil (Forsberg, 2021). Therefore the strength of the columns is closely connected to the soil type, the natural water content, the binder material as well as the mixing process. Out of these the ratio between binder and water content, as well as the soil type, are the major contributing components to the final stabilisation effect. Carlsten (1996) presents values of the stabilisation effect, S_{eff}, for different types of soil. S_{eff} is the quotient between the shear strength of the stabilised and unstabilised soil. The value of the stabilisation effect varies with soil type as well as the amount and type of binder. For clay, the stabilisation effect is high, with an S_{eff} normally between 10-20. The effect is similar for silty clay, where the S_{eff} varies between 10-30 (Larsson, 2006). Both lime and lime-cement work for clay and silty clay, but with increasing silt content lime-cement columns become more suitable. Between 80-110 kg/m^3 binding material is normally needed for lime-cement columns installed in clay. As mentioned, the mixing is also of importance. If a column is poorly mixed

discs of harder material, with softer material in between, can be formed (Larsson, 2006). These columns can hold relatively high vertical loads but are limited in their ability to restrain shear stress, tension stress and bending loads. Sometimes these weaker layers occur also in well mixed columns, due to natural variations in the soil.

During the column installation, a mixing tool is used and driven down into the soil, churning the soil as it is pushed down (Carlsten, 1996). The binder is added and mixed with the soil either as the mixing tool is pushed down or pulled up. In Sweden the binder is usually added as the tool is withdrawn from the ground, see Figure 2.1. The rotational speed used when installing lime-cement columns varies between 150-200 revolutions/min and the withdrawal rate is 15-35 mm/revolution (Forsberg, 2021). This means that the rate of installation for the columns is around 2.5-6 meter column/min. The binder feed is normally stopped 0.2-0.5 meters below the ground surface to ensure that no lime is blown into the air (Carlsten, 2000). If there is a dry crust which is thicker than 1 m it is common to stop the admixture feed 0.5 m above the bottom edge of the dry crust. Due to this, and the fact that the quality of the columns usually are uneven at the top, full strength should only be considered 1 m below the ground surface. In the beginning of the installation of the columns the strength increases rapidly and is thereafter developed at a constant rate (Carlsten, 1996). However, the strength development can be delayed in the upper sections of the columns if they are installed during low temperatures. If a faster increase of the column strength is wanted, this can be established by loading the columns directly after installation.

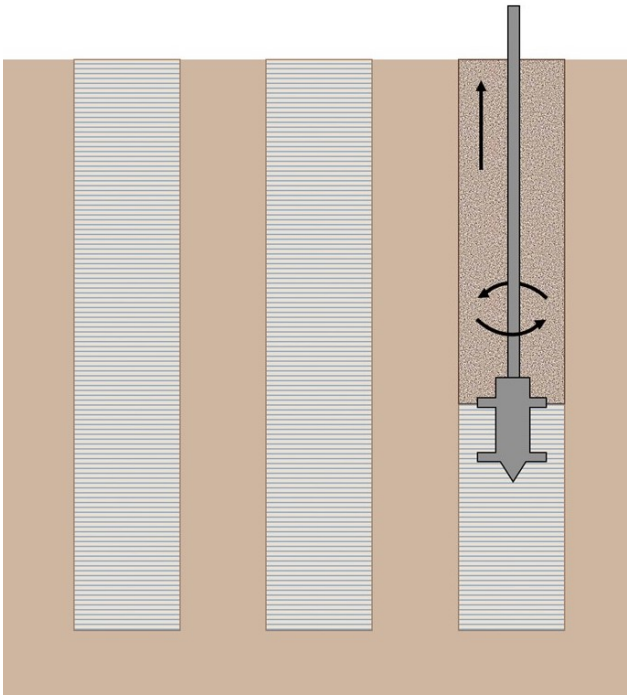

Figure 2.1: Installation of deep mixed column. Figure by the authors.

Two different methods can be used when producing deep mixed columns, the dry method or the wet method (Larsson, 2006). The dry method, which is most com-

monly used in Sweden, is suitable for soft soils with a high natural water content. The method uses compressed air to blow the binder into the soil, and the binder reacts with the natural water in the ground. On the contrary, the wet method is suitable for soils with a lower water content. When using the wet method the binding material is mixed with water before being pumped into the soil. A benefit of the wet method is that it simplifies mixing cement into the soil. If cement is being mixed in using the dry method, more extensive mixing is required compared to when using lime only. If the water content in the soil is low, a variant of the dry method can be used. With this variant water is blown into the soil at the same time as the dry binding material is mixed in.

The geometry of the columns varies based on the soil profile and the need for stabilisation. The diameter of the columns usually vary between 0.5 m and 0.8 m (Karlsson & Moritz, 2014), but in Sweden the most commonly used diameter is 0.6 m (Larsson, 2006). The length of the columns is dependent on the soil conditions, however the maximum length is usually 25 m (Topolnicki, 2016). If the depth of the soil in need of stabilisation is less then 3 m, deep mixed columns are not suitable. Furthermore, the deep mixed columns can be installed in many different patterns and both as singular or overlapping columns (EN 14679, 2005). In Figure 2.2 two common singular patterns are presented.

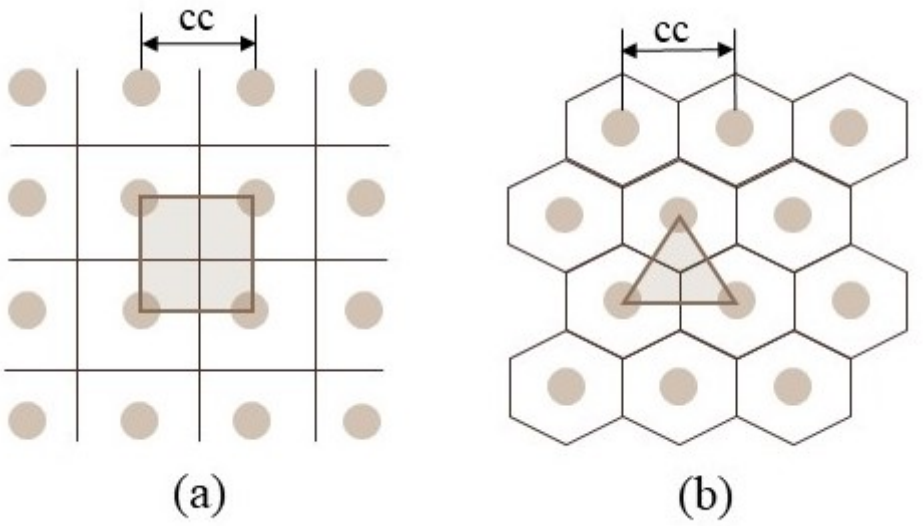

Figure 2.2: Column patterns, (a) Square, (b) Triangular (EN 14679, 2005).

As with any stabilisation method, the use of lime or lime-cement columns comes with both advantages and limitations. One advantage of the technique is its flexibility, the distance between the columns as well as the column diameter and length can be chosen to match the stabilisation problem (Carlsten, 2000). Furthermore, the columns have become both an economically and technically competitive method (Baker et al., 2005). Lime and lime-cement columns work well for clay as described above, however, lime has close to no stabilising effect if the soil is high in organic content (more than 6%) or has a high water content (more than 120%) (Carlsten,

1996). Another limitation with the method is the penetration capacity, which is limited by hard surfaces such as dry crust, roots, stones and ground frost. The installation of the columns can also cause stability problems if the ground level or rock level is inclined, as excess pore pressures are generated. The mixing tool also creates some stability problems, due to its shape, by creating a disturbed zone around 0.5 m below the bottom of the installed column. A final limitation is that some spacing of the columns can cause heave due to a volume increase when mixing in the binder material.

2.2 Constitutive Models

In the following chapter the constitutive models used in Plaxis 2D are described. The Volume Averaging Technique (VAT) uses a combination of the two models S-CLAY1S and MNhard. S-CLAY1S is used to describe the stress-strain response of clay and MNhard is used for the deep mixed columns. Furthermore, the Mohr-Coulomb model is used for the dry crust and embankment.

2.2.1 S-CLAY1S

The S-CLAY1S model is based on the isotropic Modified Cam-clay model, developed by Roscoe and Burland (1968), and is further an extension of the anisotropic S-CLAY1 model proposed by Wheeler (1997). In comparison to these two models, S-CLAY1S also takes into account anisotropy and bonding between soil particles as well as the degradation of these bonds (Koskinen et al., 2002).

Anisotropy, bonding and destructuration are fundamental soil behaviours often seen in natural clays where the latter is especially prominent in sensitive clays (Sivasithamparam et al., 2015). The anisotropic behaviour of clays originates from the consolidation and deposition history as well as the plate-like shape of the clay particles (Karstunen & Koskinen, 2008). While anisotropy can be seen in both the elastic and plastic behaviour of the soil, the plastic anisotropy dominates in most loading problems for normally consolidated and lightly overconsolidated clays (Karstunen et al., 2006). This applies for embankment problems, where the plastic strains are significantly larger compared to the elastic strains. In the S-CLAY1S model, anisotropy is taken into account through an inclination of the yield surface, corresponding to the inclined yield surface of natural clays seen in experiments (Becker & Karstunen, 2013).

Bonding between soil particles provides the soil with additional strength and yield resistance (Karstunen et al., 2005). During plastic straining of the soil, the soil particles and the contacts between them are rearranged. This results in the inter-particle bonds gradually being destroyed, a process which is called destructuration. The additional yield resistance provided by the inter-particle bonding can for example be seen in oedometer tests on natural bonded and reconstituted (unbounded) clays, seen in Figure 2.3 (Karstunen et al., 2006). The curve of the natural clay exhibits a higher preconsolidation pressure compared to the curve of the unbonded

or intrinsic clay. In Figure 2.3 it can also be seen that the curve of the bonded clay gradually approaches the intrinsic curve as a result of the gradual degradation of the inter-particle bonding.

Bonding and destructuration are considered in S-CLAY1S through the inclusion of an additional smaller intrinsic yield surface, firstly proposed by Gens and Nova (1993). The intrinsic yield surface represents the soil behaviour when all particle bonds have been destroyed and has the same inclination and shape as the yield surface of the bonded soil. The difference in size between the two yield surfaces represents the effect of the inter-particle bonding.

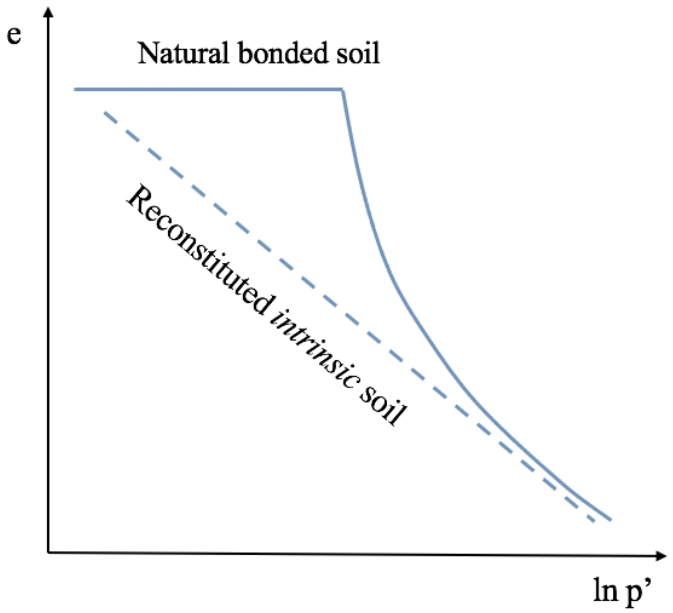

Figure 2.3: Compression curve from Oedometer test for a natural (bonded) soil and a reconstituted intrinsic soil. Figure after Karstunen et al. (2006).

The yield surface of the S-CLAY1S model appears as an ellipsoid when plotted in the three dimensional stress space, visualised in Figure 2.4. As a simplification, the yield surface can additionally be explained in the triaxial stress space as a function of the deviator stress q and the mean effective stress p', see Figure 2.4. The simplified case is only valid for soils exposed to triaxial or oedometric loading and where the soil and stress state are cross-anisotropic (Karstunen & Koskinen, 2008). Cross-anisotropy is often seen in soil and rock and is characterised by an anisotropic behaviour in the direction perpendicular to the layering of the material, within which the behaviour is isotropic (Gao et al., 2010). The yield surface in the triaxial stress space is further described by Equation 2.1 (Koskinen et al., 2002):

$$f = (q - \alpha p')^2 - (M_c^2 - \alpha^2)(p'_m - p')p' = 0 \tag{2.1}$$

where M_c denotes the critical state stress ratio. The parameter α describes the amount of anisotropy and represents the inclination or the orientation of the yield

surface. The size of the yield surface is represented by the parameter p'_m, where the size of the bonded yield surface is related to the size of the unbonded intrinsic yield surface, p'_{mi}, through Equation 2.2:

$$p'_m = (1 + x)p'_{mi} \tag{2.2}$$

where the parameter x is connected to the difference in size between the bonded and the unbonded yield surface and represents the amount of bonding.

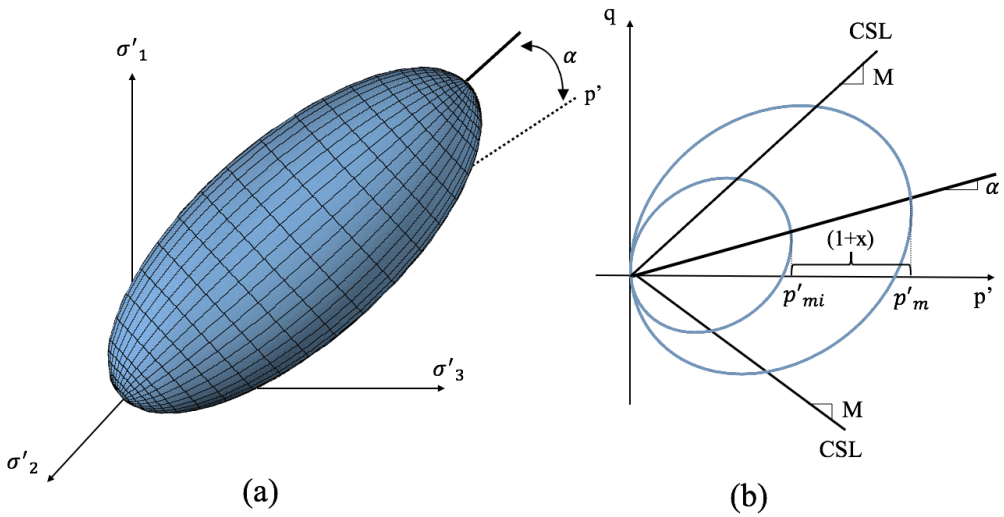

Figure 2.4: Yield surface of the S-CLAY1S model in, (a) 3D stress space, (b) Triaxial stress space. Figure after Karstunen et al. (2005).

As a simplification, the elastic response of the soil is assumed to be isotropic in the S-CLAY1S model, following the formulation of the Modified Cam-clay model (Karstunen et al., 2006). The model further assumes an associated flow rule. An associated flow rule implies that the plastic potential, or the direction of the change in plastic deformations ($d\varepsilon^p$), is related to the yield surface i.e. the increase of plastic strain is determined from the yield function (Vogler, 2008). The flow rule can also be non-associated, meaning that the plastic potential function, expressing the increase of plastic strain, differs from the yield function, see Figure 2.5. Using an associated flow rule can result in the dilatancy being inaccurately predicted for granular soils, this especially applies when the Drucker Prager or the Mohr Coulomb yield criteria is used. Investigations on clay, for example by Graham et al. (1983), have shown that the increase of plastic strain is practically normal to the yield surface (when no kinematic hardening is considered), justifying the use of an associated flow rule in the S-CLAY1S model.

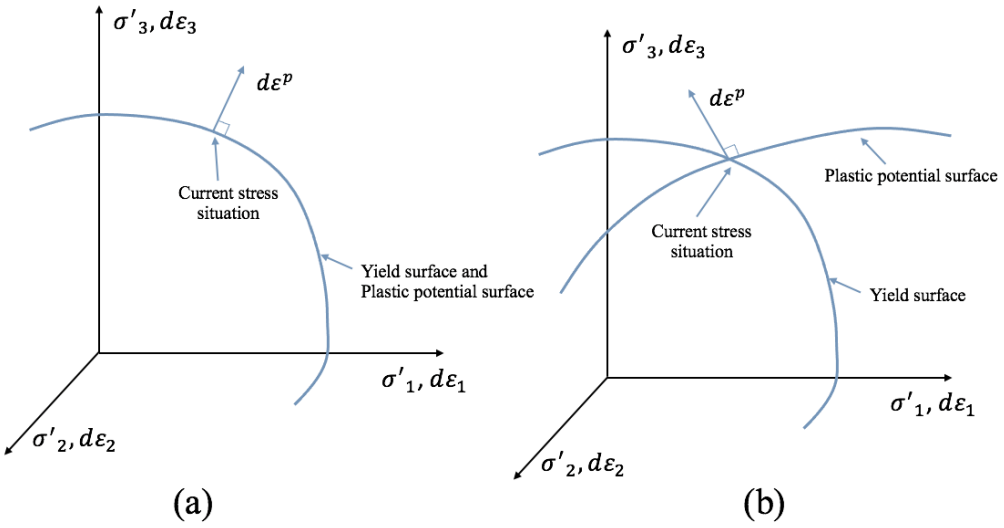

Figure 2.5: (a) Associated flow rule, (b) Non-associated flow rule. Figure after Vogler (2008).

S-CLAY1S includes three hardening laws (Koskinen et al., 2002). The first hardening law relates the plastic volumetric strain increment, $d\varepsilon_v^p$, to the increase in size of the unbonded intrinsic yield surface. The hardening law is based on the assumption that an increase of the yield surface for an unbonded soil is due only to the soil particles rearranging into a denser soil volume, something which occurs during plastic straining. The first hardening law is described by Equation 2.3:

$$dp'_{mi} = \frac{(1+e)p'_{mi}}{\lambda_i - \kappa} d\varepsilon_v^p \tag{2.3}$$

where e denotes the void ratio and λ_i and κ denotes the intrinsic compression index and the swelling index in the e - $ln\ p'$ space respectively.

Plastic straining changes the anisotropy of the soil as the soil particles are rearranged (Karstunen & Koskinen, 2008). The behaviour is incorporated in the second hardening law of the S-CLAY1S model which describes the rotation of the yield surface in relation to the incremental plastic strain and is described by Equation 2.4:

$$d\alpha = \mu \left[\left(\frac{3\eta}{4} - \alpha \right) \left\langle d\varepsilon_v^p \right\rangle + \beta \left(\frac{\eta}{3} - \alpha \right) \left| d\varepsilon_d^p \right| \right] \tag{2.4}$$

where μ denotes the absolute rate of change of the yield surface inclination, $d\alpha$, as it rotates towards the existing target value. The target value of $d\alpha$ is dependent on the current stress state, represented by the η parameter ($\eta = \frac{q}{p'}$). The rotation of the yield surface is further dependent on both the plastic volumetric strain ($d\varepsilon_v^p$),

influencing $d\alpha$ towards a value of $\frac{3\eta}{4}$, and the plastic shear strain ($d\varepsilon_d^p$), influencing $d\alpha$ towards a value of $\frac{\eta}{3}$ (Koskinen et al., 2002). The β parameter determines the shear and volumetric strains' effectiveness in rotating the yield surface.

The third hardening law, Equation 2.5, describes the destructuration behavior of a soil subjected to plastic straining, where the inter-particle bonding is gradually destroyed (Koskinen et al., 2002):

$$dx = -ax\Big(\Big|d\varepsilon_v^p\Big| + b\Big|d\varepsilon_d^p\Big|\Big) \tag{2.5}$$

where x represents the amount of bonding and is assumed to be reduced by both plastic shear and volumetric strains and decreases towards a target value of zero. Hence, as the destructuration process progresses, the yield surface of the natural clay and the intrinsic yield surface will approach each other until they coincide (Vogler, 2008). Given the hardening laws of the S-CLAY1S model, it could be that the intrinsic yield surface will increase as a result of the volumetric hardening, and the yield surface of the natural clay will reduce as a result of destructuration. Moreover, the parameter a describes the absolute rate of the destructuration and b describes the shear and volumetric strains' relative effectiveness in degrading the inter-particle bonding.

As previously mentioned, the S-CLAY1S model is based on the Modified Cam-clay and the S-CLAY1 model and the S-CLAY1S can easily be reduced to these two models by modifying some of the input parameters in the model (Karstunen & Koskinen, 2008). By putting the initial value of the bonding parameter, x_0, to zero and using the λ for the natural bonded soil instead of the intrinsic value, S-CLAY1S is reduced to the S-CLAY1 model. By further putting the initial inclination of the yield surface, α_0 and the μ parameter to zero, the model is reduced to the isotropic Modified Cam-clay model (Karstunen et al., 2006).

The input parameters required in the S-CLAY1S model is presented in Table 2.1.

Table 2.1: Input parameters for the S-CLAY1S model.

Parameter	Description
κ	Swelling index in e - ln p' space
ν'	Poisson's ratio
λ_i	Intrinsic compression index in e - ln p' space
M_c	Critical state stress ratio
μ	Absolute rate of change of yield surface inclination
β	Effectiveness of yield surface rotation
a	Absolute rate of destructuration
b	Relative effectiveness of destructuration
OCR	Over consolidation ratio
POP	Pre overburden pressure
e_0	Initial void ratio
α_0	Initial yield surface inclination
x_0	Initial amount of bonding

2.2.2 MNhard

The MNhard model was developed by Benz (2007) and is an adaptation of the hardening soil (HS) model. It implements the yield criterion which Matsuoka and Nakai developed in the early 1980's (Vogler, 2008). A benefit with the Matsouka-Nakai yield criterion is that it is more similar to the observed experimental yield surface of granular soils compared to the commonly used Mohr-Coulomb criterion, see Figure 2.6. In addition, the smoother yield surface achieved when using the MN yield criterion also makes the model more computationally convenient (Bower et al., 2020). Another advantage is that the MN yield criterion considers the impact of the intermediate principal stress on the strength of the material.

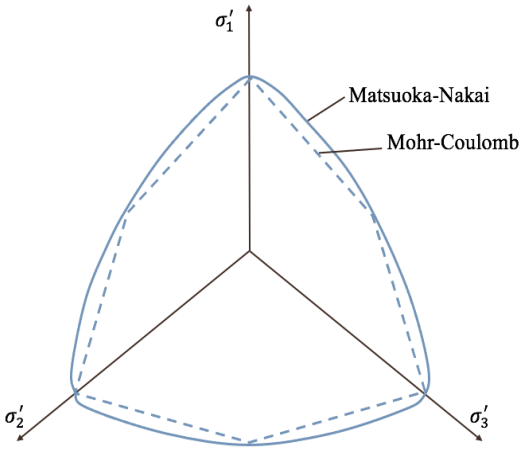

Figure 2.6: The Mohr-Coulomb and Matsuoka-Nakai yield criterion in the octahedral space. Figure after Vogler (2008).

The Matsuoka-Nakai yield function is given by Equation 2.6:

$$f = \frac{3}{2}\frac{1}{E_{50}}\frac{\left(\frac{1-sin\phi'_m}{sin\phi'_m}\right)}{\left(\frac{1-sin\phi'_m}{sin\phi'_m}\right) - R_f\left(\frac{1-sin\phi'}{sin\phi'}\right)} - \frac{3}{2}\frac{q}{E_{ur}} - \gamma_s^{ps} = 0 \tag{2.6}$$

where the hardening parameter γ_s^{ps} is the objective shear strain (Benz, 2007). The mobilised friction angle is denoted with ϕ'_m and R_f denotes the failure ratio between the ultimate deviatoric stress and the asymptote of the hyperbolic stress strain relation. According to Brinkgreve and Vermeer (2021), a default value of 0.9 is set for R_f.

The MNhard model is a hardening plasticity model, meaning that the yield surface is not fixed in the principal stress space and it can therefore expand due to plastic straining (Vogler, 2008). In the model shear hardening is implemented by a non-associated flow rule and it is used to model the irreversible strains which occur due to the primary deviatoric loading. The other main type of hardening, volumetric hardening, is used to model irreversible strains which exist due to isotropic loading as well as one-dimensional loading. This type of one-dimensional loading is considered to be of small importance for deep mixed columns. Therefore, as a simplification, it is not implemented in the MNhard model. In contrast to the original HS model, MNhard has been reformulated to be dependent on the Lode angle, θ (Benz et al., 2008), a parameter indicating how the the size of the intermediate principal stress, σ_2, relates to the major and minor principal stresses, σ_1 and σ_3 (Danas et al., 2012). This reformulation allows for more smoother yield criterions, like Matsuoka-Nakai, to be included in the model (Benz et al., 2008). The MNhard model does not account for rotation of principle stresses, initial anisotropy or stress induced anisotropy.

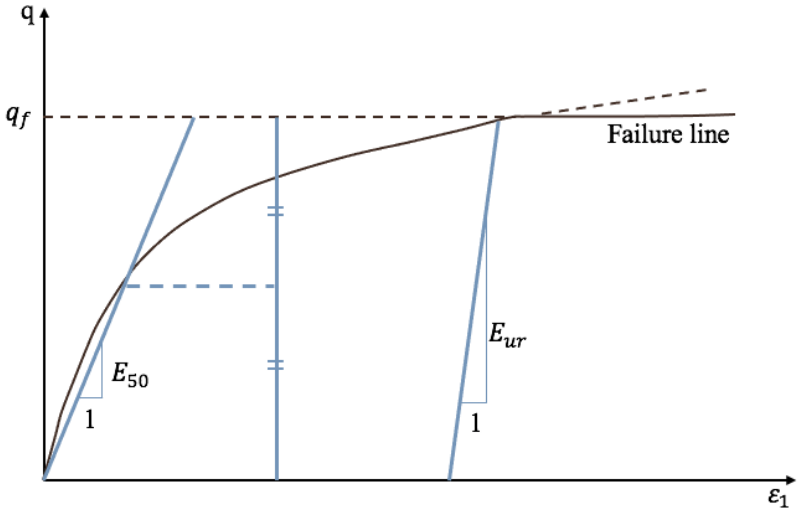

Figure 2.7: The Hyperbolic stress-strain relationship for a standard drained triaxial test in primary loading. Figure after Vogler (2008).

Lime-cement columns exposed to primary triaxial loading usually display a hyperbolic relationship between vertical strain, ε_1 and deviatoric stress, q (Vogler, 2008), as seen in Figure 2.7. This relationship is included in the MNhard model and is defined by the secant elasticity modulus, E_{50} (Becker & Karstunen, 2013). E_{50} is stress dependent and can therefore also be calculated with Equation 2.7:

$$E_{50} = E_{50}^{ref} \left(\frac{c' cos\phi' + \sigma_3' sin\phi'}{c' cos\phi' + p_{ref}' sin\phi'} \right)^m \tag{2.7}$$

where m denotes the amount of stress dependency. The dependency varies between 0.5-1.0 for clays and dense sands. The value of m increases if the material is denser or overconsolidated.

The modulus for unloading/reloading, E_{ur} is by default set as three times E_{50} (Brinkgreve & Vermeer, 2021). E_{50} can also be determined graphically as shown in Figure 2.7. This makes it possible to rearrange Equation 2.7 to determine E_{50}^{ref}, the reference stiffness modulus at the reference stress p_{ref}' (Vogler, 2008). The reference elasticity modulus is used to calculate the shear modulus, G, which is used as input in the Plaxis MNhard model. Shear modulus is calculated from the relationship with E and Poisson's ratio at drained conditions, ν', as shown in Equation 2.8 (Knappett & Craig, 2012).

$$G = \frac{E}{2(1+\nu')} \tag{2.8}$$

All needed input parameters for the MNhard model is shown in Table 2.2.

Table 2.2: Input parameters for the MNhard model.

Parameter	Description
c'	Effective cohesion
ψ'	Effective dilatancy angle
ϕ'	Effective friction angle
G_{ur}^{ref}	Reference shear modulus for unloading/reloading
ν'	Poisson's ratio at drained conditions
m	Power of hyperbolic stress-strain law
p_{ref}'	Reference pressure for hyperbolic stress-strain law
R_f	Ratio of failure
f_t	Allowable tensile stress
G_{50}^{ref}	Reference shear modulus for primary loading
Skempton-B	Skempton-B for undrained loading

2.2.3 Mohr-Coulomb

The Mohr-Coulomb model is an elastic-perfectly plastic model (Mohsan et al., 2021), based on the theories presented by Charles-Augustin de Coulomb and Otto Mohr in 1773 and 1900 (Yu, 2002). The elastic part of the model follows Hooke's law and assumes a linear-elastic stress-strain response (Mohsan et al., 2021). The plastic part of the model is based on the Mohr-Coulomb failure criterion, which is formulated by Equation 2.9 as a function of the principal stresses σ'_1 and σ'_3 (Knappett & Craig, 2012).

$$f = (\sigma'_1 - \sigma'_3) - (\sigma'_1 + \sigma'_3)sin\phi' + 2c'cos\phi' = 0 \tag{2.9}$$

In 2D, the Mohr-Coulomb failure criterion is further described according to Figure 2.8, where the stress state is represented by a Mohr circle (Knappett & Craig, 2012). Failure occurs when the circle touches the failure envelope, expressed by Equation 2.9, and a stress state located above the failure envelope is therefore not possible. In the three-dimensional principal stress state, the Mohr-Coulomb failure criterion is expressed as a hexagonal cone, visualised in Figure 2.9 (Labuz & Zang, 2012). In Figure 2.9 the cross-section of the failure criterion by an octahedral plane is also presented, previously seen in Section 2.2.2. The angular shape of the failure surface produces some complications during numerical computations of the model due to discontinuities at the edges and tips of the surface (Xiang & Zi-Hang, 2017).

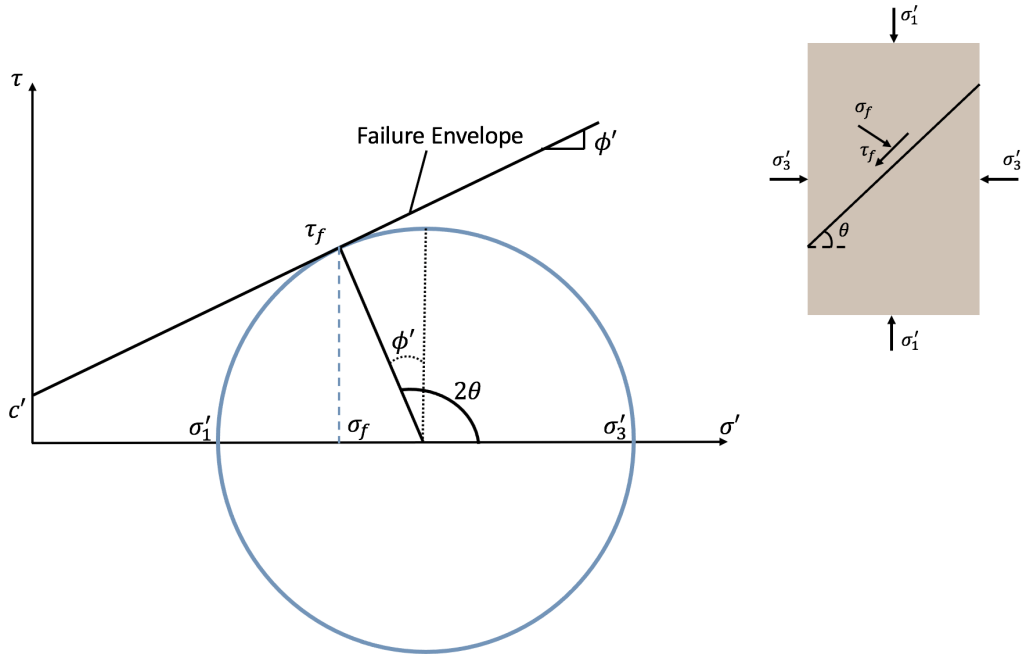

Figure 2.8: Mohr-Coulomb failure criterion in two dimensions. Figure after Knappett and Craig (2012).

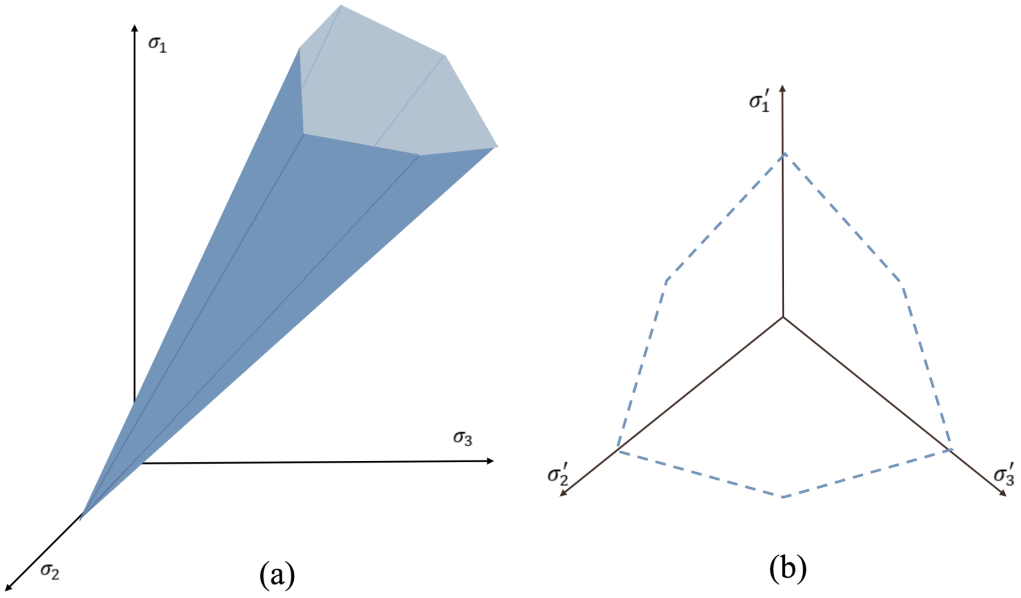

Figure 2.9: Mohr coulomb failure criterion in (a) principal stress state (b) the octahedral plane. Figure after Labuz and Zang (2012).

The parameters required in the Mohr-Coulomb model is presented in Table 2.3 below. In Plaxis, the shear modulus, G, and the Oedometer modulus, E_{oed}, can be set as alternative stiffness parameters to the Young's modulus, E (Brinkgreve & Vermeer, 2021).

Table 2.3: Input parameters for the Mohr-Coulomb model.

Parameter	Description
E	Young's modulus
ν	Poisson's ratio
G	Shear modulus
E_{oed}	Oedometer modulus
c	Cohesion
ϕ	Friction angle
ψ	Dilatancy angle
σ_t	Tension cut-off and tensile strength

2.2.4 Volume Averaging Technique

Volume Averaging Technique (VAT) is a homogenisation technique used for deep mixed columns and soft soil (Vogler, 2008). The technique uses the constitutive models for each material and averages them into one model. If the two materials are modelled separately, three-dimensional calculations are needed and each individual column needs a large number of volume elements. Additionally, to allow for accurate prediction of the stress distribution between soil and column, a higher mesh fineness is needed, increasing the number of elements further. However, by modelling the two materials as one composite material instead of two individual ones,

the geometric discretisation is considerably simplified from a three-dimensional problem to a two-dimensional problem, see Figure 2.10. This simplification results in a significant reduction in calculation costs and it will also enable the possibility to model problems involving a large number of columns. The VAT model is suitable for designing periodically reinforced soils since the spacing between columns and the column diameter easily can be changed without the need of a new discretisation. The finite element mesh is also simpler, since the columns are smeared over the whole domain, meaning that the mesh is not dependent on the spacing and diameter of the columns. The constitutive models used for the two materials can vary, any elasto-plastic model will work. For this problem, the S-CLAY1S model is used for the soil and the MNhard model is used for the columns.

The VAT model is based on the homogenisation technique for the axisymmetric problem of a unit cell developed by Lee and Pande (1998). In the model by Lee and Pande, individual stiffness matrices for each of the constituents weighted by the corresponding volume fractions are used to develop an equivalent elastic material stiffness matrix. However, their proposed approach has a major drawback (Vogler, 2008); stresses that are not in equilibrium are adjusted without considering the influence on the strain distribution between the two constituents. Therefore, an additional approach has been used for the VAT model. This approach is based on the idea presented by Schweiger in 1989 which updates the strain distribution in an iterative process until equilibrium is achieved (Vogler, 2008). Additionally, the used finite-element code has an unique pore pressure value in each integration point. This means that the soil and columns have the same excess pore water pressure in each point during the consolidation process. This implementation does thereby not allow for individual permeabilities for the soil and column material.

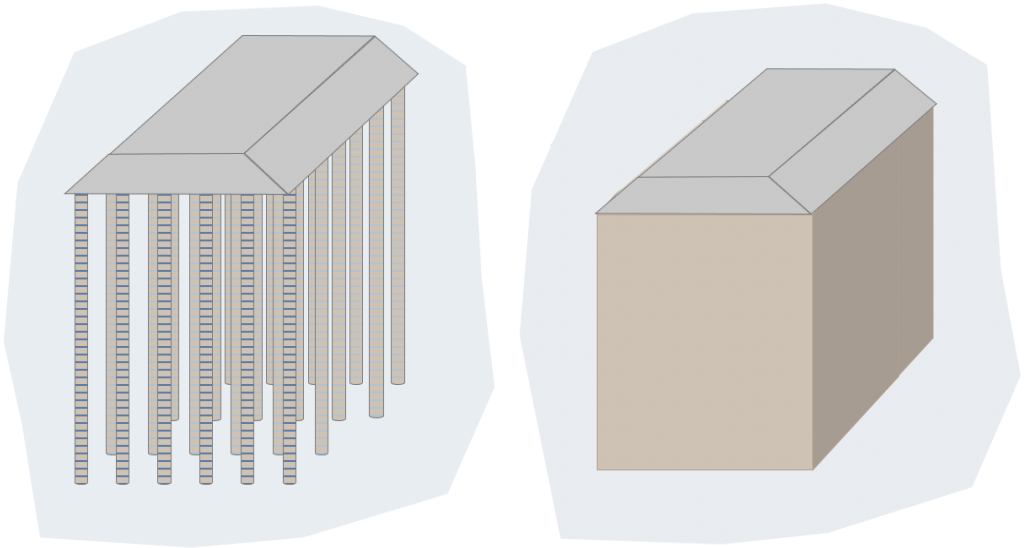

(a) (b)

Figure 2.10: (a) Discrete and (b) homogenised visualisation of columns under an embankment. Figure after Vogler (2008).

The VAT model is based on several assumptions, the first being that the columns are homogeneous and uniformly distributed over the reinforced region (Vogler, 2008). This means that the two constituent materials exist simultaneously in the whole region and it is what allows the two materials to be modelled as one. However, it should be mentioned that the assumption is not very accurate if very few columns are used for reinforcement. Another assumption, which is a result of the first assumption, is that the vertical strain is the same for the two materials. It is further assumed that the two constituents are perfectly bonded, resulting in the soil and column having both the same vertical and horizontal shear deformations, as presented in Equation 2.10. In the equation the homogenised material, consisting of soil (s) and column (c), is denoted as *eq*. To reach equilibrium between the two constituents regarding radial stresses, radial strains between the soil and columns are allowed.

$$\begin{aligned} \dot{\varepsilon}_y^{eq} &= \dot{\varepsilon}_y^s = \dot{\varepsilon}_y^c \\ \dot{\gamma}_{zx}^{eq} &= \dot{\gamma}_{zx}^s = \dot{\gamma}_{zx}^c \end{aligned} \tag{2.10}$$

Furthermore, it is guaranteed that stress equilibrium at the boundary between soil and column is reached, in regards to radial and shear stresses, as presented in Equation 2.11 (Vogler, 2008). This is ensured even though the boundary is reduced to a virtual one in the VAT model. An assumption is also made regarding the constitutive stress-strain relationship between the soil and columns. It is assumed that the relationship will not be violated and individual yield functions, stiffness matrices and hardening laws can therefore be defined for each material. As mentioned before, the VAT model also assumes that both the unimproved and improved soil have the same hydraulic conductivity. The binder type, mixing process and in-situ soil affects the accuracy of this assumption.

$$\begin{aligned} \dot{\sigma}_x^{eq} &= \dot{\sigma}_x^s = \dot{\sigma}_x^c \\ \dot{\sigma}_z^{eq} &= \dot{\sigma}_z^s = \dot{\sigma}_z^c \\ \dot{\tau}_{xy}^{eq} &= \dot{\tau}_{xy}^s = \dot{\tau}_{xy}^c \\ \dot{\tau}_{yz}^{eq} &= \dot{\tau}_{yz}^s = \dot{\tau}_{yz}^c \end{aligned} \tag{2.11}$$

The VAT model implements both the Voigt assumption and the Reuss assumption (Vogler, 2008). The Voigt assumption is applied in the axial direction of the columns and assumes that the strains are the same throughout the stabilised soil, with perfect bonding between the two constituents. The Reuss assumption is applied radial to the columns, it assumes that the stresses within each constituent are the same throughout the stabilised soil. Both assumptions have errors, for the Voigt assumption no equilibrium is reached between the tractions at the boundaries

between column and soil. With the Reuss assumption the soil and column matrix will not be bonded.

As mentioned a homogeneous and uniform distribution of columns is assumed in the VAT model (Vogler, 2008). The volume ratios, Ω, for both column and soil are defined as presented in Equation 2.12:

$$\Omega_c = \frac{A_c}{A} \qquad \Omega_s = \frac{A_s}{A} \tag{2.12}$$

where A_c is the cross-sectional area for the columns and A_s is the same for the soil. A denotes the total area and is the sum of the two cross-sectional areas.

The volume ratios are used to determine the stress and strain increment for the homogenised material (Becker & Karstunen, 2013). It is done according to Equation 2.13 and 2.14:

$$\dot{\boldsymbol{\sigma}}^{\boldsymbol{eq}} = \Omega_c \dot{\boldsymbol{\sigma}}^{\boldsymbol{c}} + \Omega_s \dot{\boldsymbol{\sigma}}^{\boldsymbol{s}} \tag{2.13}$$

$$\dot{\boldsymbol{\varepsilon}}^{\boldsymbol{eq}} = \Omega_c \dot{\boldsymbol{\varepsilon}}^{\boldsymbol{c}} + \Omega_s \dot{\boldsymbol{\varepsilon}}^{\boldsymbol{s}} \tag{2.14}$$

where $\dot{\boldsymbol{\sigma}}$ denotes the stress rate tensors and $\dot{\boldsymbol{\varepsilon}}$ the strain rate tensors.

In Equation 2.15 and 2.16 the constitutive laws of the soil and column are described with regards to increments of effective stress (Vogler, 2008):

$$(\dot{\boldsymbol{\sigma}}^{\boldsymbol{s}})' = \boldsymbol{D}^{\boldsymbol{s}} \dot{\boldsymbol{\varepsilon}}^{\boldsymbol{s}} \tag{2.15}$$

$$(\dot{\boldsymbol{\sigma}}^{\boldsymbol{c}})' = \boldsymbol{D}^{\boldsymbol{c}} \dot{\boldsymbol{\varepsilon}}^{\boldsymbol{c}} \tag{2.16}$$

where $\boldsymbol{D}$ denotes the stiffness matrices of each of the materials. Further, with respect to the previously presented relationship to the homogenised material, a constitutive law for the material can be formulated as in Equation 2.17:

$$(\dot{\boldsymbol{\sigma}}^{\boldsymbol{eq}})' = \boldsymbol{D}^{\boldsymbol{eq}} \dot{\boldsymbol{\varepsilon}}^{\boldsymbol{eq}} \tag{2.17}$$

$\boldsymbol{D^{eq}}$ denotes the stiffness matrix of the homogenised material which can be defined as presented in Equation 2.18 (Vogler, 2008):

$$\boldsymbol{D^{eq}} = \Omega_s \boldsymbol{D^s S_1^s} + \Omega_c \boldsymbol{D^c S_1^c} \tag{2.18}$$

where **S** is the relations of the strain increments between the soil and column.

When implementing VAT into Plaxis 2D an implicit backward Euler integration scheme (Vogler & Karstunen, 2009) is used. Due to this and the highly non-linear behaviour of both materials, a sub-iteration scheme is also necessary. In this project VAT is applied into Plaxis with an userdefined model (Abed et al., Submitted). The input data used in the model is the parameters for both S-CLAY1S and MNhard presented previously. Some additional parameters are added, these are presented in Table 2.4.

Table 2.4: Additional input parameters for the VAT model.

Parameter	Description
Stepsize	Increment size of sub-iteration
Ω_c	Column volume ratio
$init_{strain_{reduce}}$	Initial strain reduction

3
Derivation of Input Data

3.1 Soil Parameters

The Nödinge test site is located in the Göta River valley north of Gothenburg (Olsson et al., 2008). In similarity with other sites in the valley, the soil mainly consists of soft glacial and post-glacial clay. In Nödinge the stratigraphy consists of a thin dry crust on top of a thick continuous clay layer. Below the clay there is a thin layer of friction material followed by bedrock (Alén et al., 2006). In Figure 3.1 the geological layering of the soil is shown. It should be noted that neither the friction material nor the bedrock is included in the figure, this is because these layers were not included when modelling. The groundwater level and the thickness of the dry crust is chosen in accordance to Olsson (2010).

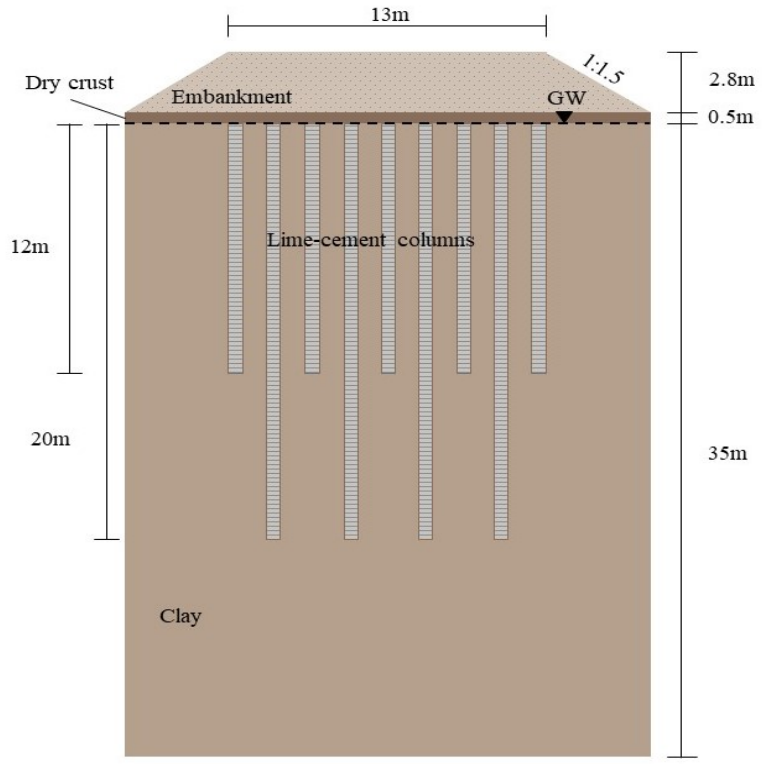

Figure 3.1: The stratigraphy of the Nödinge test site as well as the embankment and installed lime-cement columns.

For the modelling in Plaxis 2D, the continuous clay layer was divided into 6 thinner layers in order to better represent the change of the soil parameters with depth. The depth of each layer is presented in Table 3.1 below. Furthermore, the clay was modelled with undrained soil behaviour, i.e. based on effective stresses, using the S-CLAY1S model.

As part of the feasibility study and research of the Nödinge embankment, a large amount of raw data from both field tests and laboratory tests on the clay were available. However, the exact location of most of the boreholes was unknown and of the few with a known location only two, BH10010 and BH10010b, were placed close to the test embankment. Therefore, these two boreholes were the primary sources when deriving parameters for the clay layer. For both BH10010 and BH10010b, CRS tests were conducted, with a strain rate of 0.7 %/h. To get an idea of the reliability of the CRS test results, the sample quality was evaluated according to the method described by Larsson et al. (2007). As can be seen in Figure 3.2, the sample quality was considered acceptable for borehole BH10010. Hence, no corrections of these values was made. However, the tests from BH10010b are of poor quality and were therefore corrected if the results diverged from the rest of the results at a similar depth.

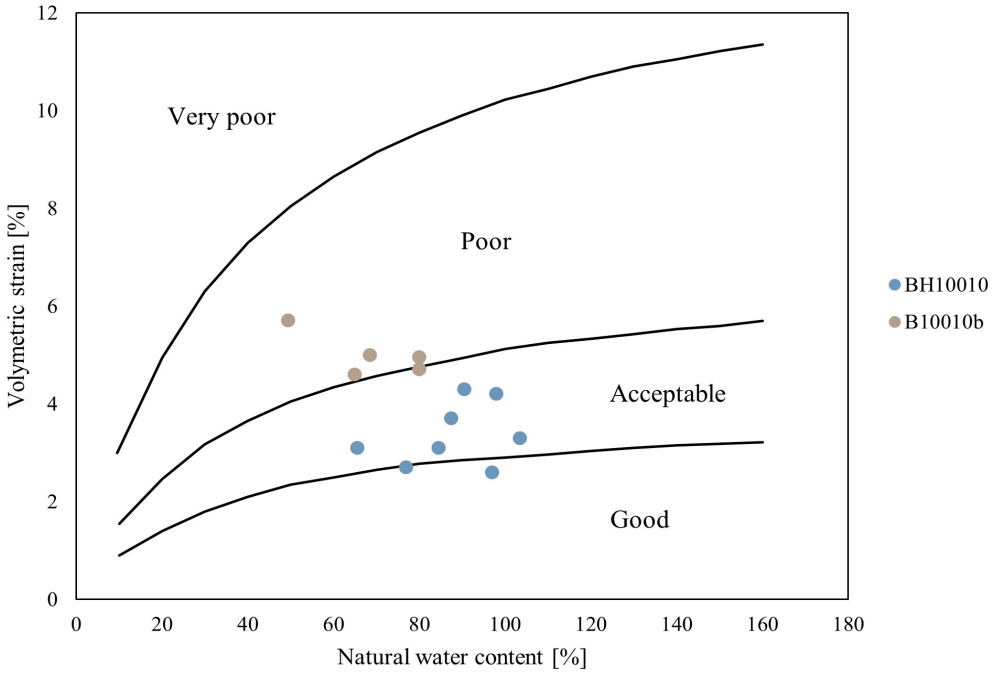

Figure 3.2: Sample quality for BH10010 and BH10010b.

The density, ρ, and initial void ratio, e_0, for borehole BH10010 are plotted in Figure 3.3 below together with values from boreholes with unknown locations. A trend line was drawn, mainly following BH10010, matching the levels of the chosen layers. No

information on density and void ratio were given for BH10010b. The density was then used to calculate the unit weight of the clay. This was done by multiplying the density with the gravitational constant which was assumed to be 10 Nm^2/kg^2.

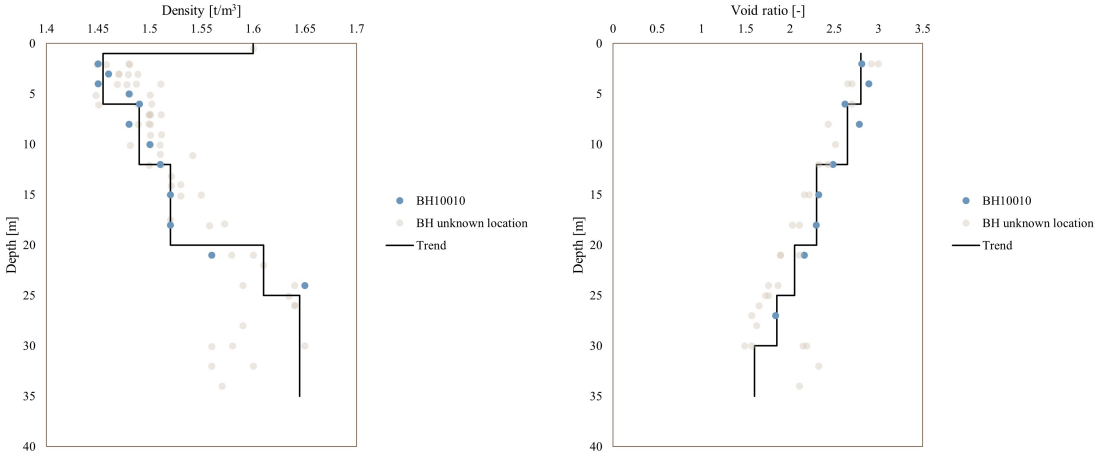

(a) (b)

Figure 3.3: (a) Density and (b) void ratio with depth for BH10010 and boreholes with unknown location.

The swelling index, κ, and compression index, λ, were retrieved from the CRS tests. It should however be noted that the tests were not loaded far enough for all particle bonds in the clay to be destroyed and the intrinsic compression index could therefore not be retrieved from the tests. Instead, the compression index for the natural bonded soil is used. In addition to this, the initial value of the bonding parameter, x_0, was put to zero. Hence, the S-CLAY1S model was reduced to a S-CLAY1 model as described previously in Section 2.2.1. The parameters κ and λ were retrieved from plots of the volumetric strain as a function of the natural logarithm of the vertical effective stress. The swelling index was determined from the initial slope of the stress-strain curve, see Figure 3.4, at a stress level corresponding to the in-situ stress level in Nödinge. The compression index was determined from the inclination at the steepest part of the stress-strain curve. From the same graph the preconsolidation pressure, σ'_c, was also determined.

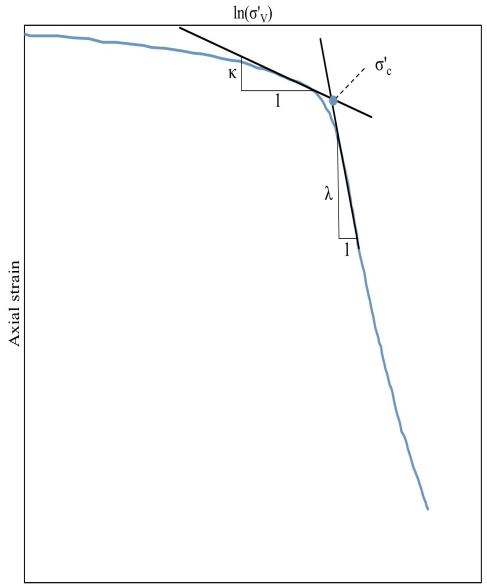

Figure 3.4: Graphic explanation of how κ, λ and σ'_c were determined.

The SoilTest facility in Plaxis was used to analyse how well the modelled soil behaviour corresponded to the results from the CRS laboratory tests. Since the model results and the laboratory test results did not match when using the values derived from the laboratory tests, the κ and λ values were altered until convergence was achieved. In Figure 3.5 the convergence of the two curves at 12 m depth for borehole BH10010 is shown, for the curves at the remaining depths and borehole BH10010b see Appendix A.

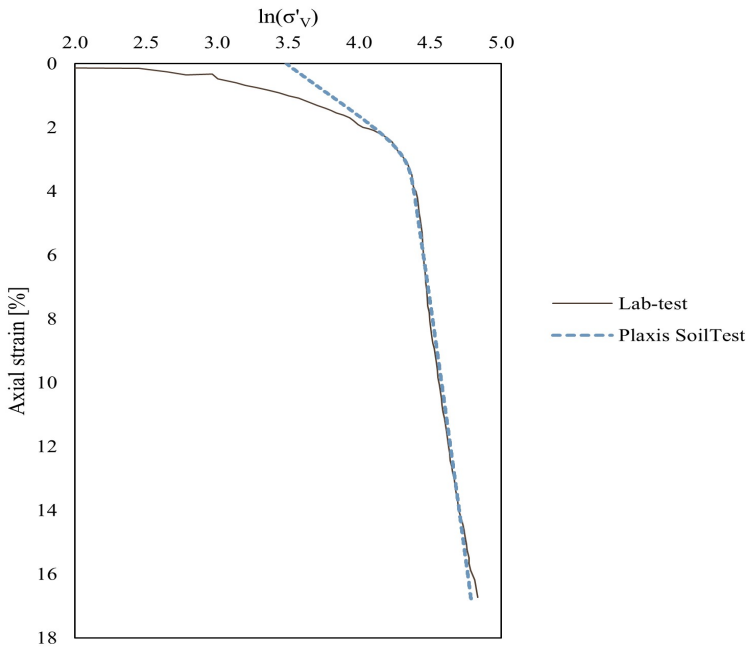

Figure 3.5: Calibration of curves from Lab-test and Plaxis SoilTest at 12m depth.

The final values of κ and λ obtained from Plaxis SoilTest facility are presented in Figure 3.6. The values for λ from borehole BH10010b were corrected to better match with values for borehole BH10010 on a similar depth, following the sample quality evaluation previously described. A trend line was drawn with respect to the chosen soil layers. The same was done for the preconsolidation pressure, which can also be seen in Figure 3.6.

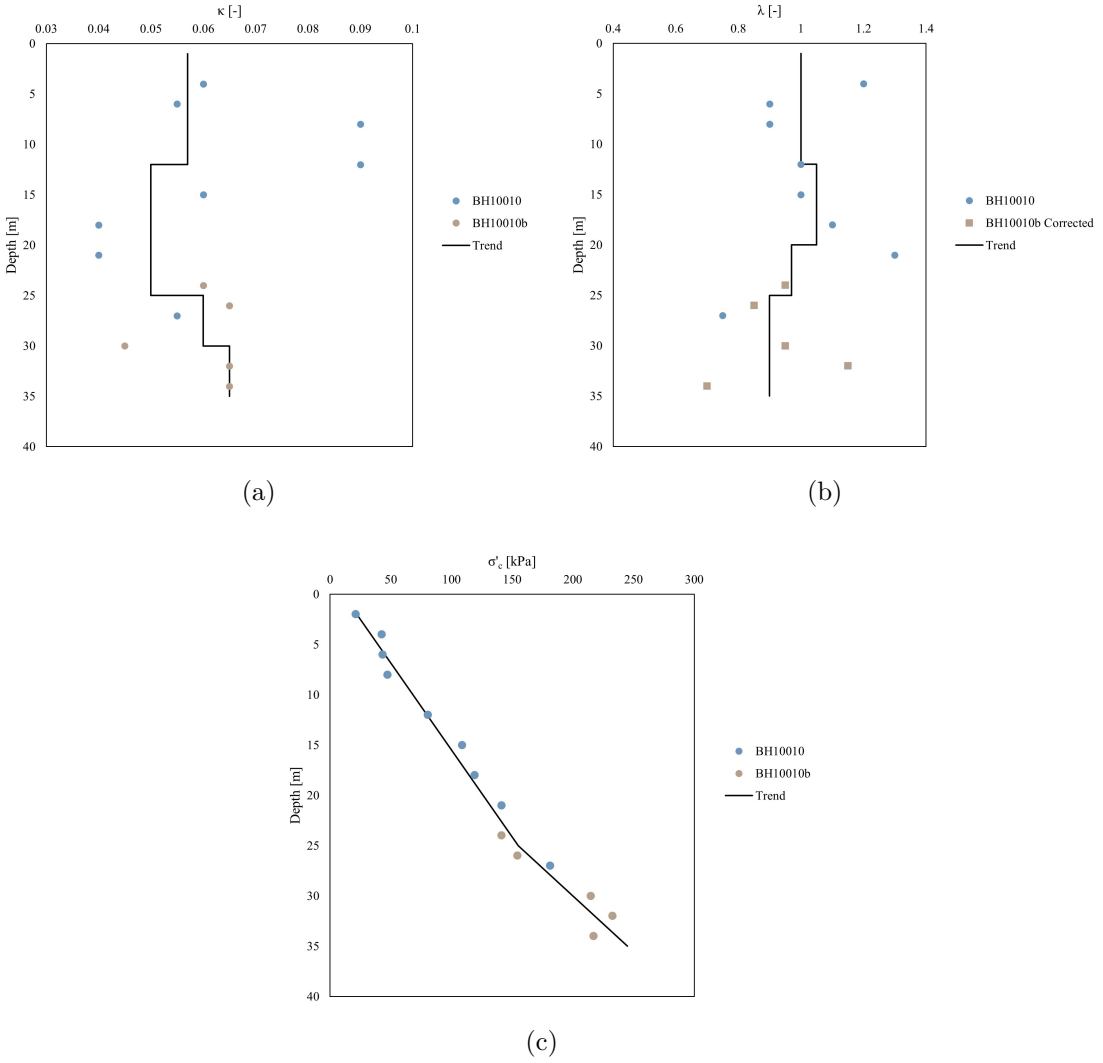

Figure 3.6: (a) Swelling index, (b) compression index and (c) preconsolidation pressure with depth for BH10010 and BH10010b.

With the preconsolidation pressure determined, the over-consolidation ratio, OCR, and the pre-overburden pressure, POP, could be calculated according to Equation 3.1 (Karstunen & Amavasai, 2017). The result of the calculation can be seen in Figure 3.7. Note that the POP is put as negative in the VAT Plaxis model.

$$OCR = \frac{\sigma'_c}{\sigma'_v}$$
$$POP = \sigma'_c - \sigma'_v \tag{3.1}$$

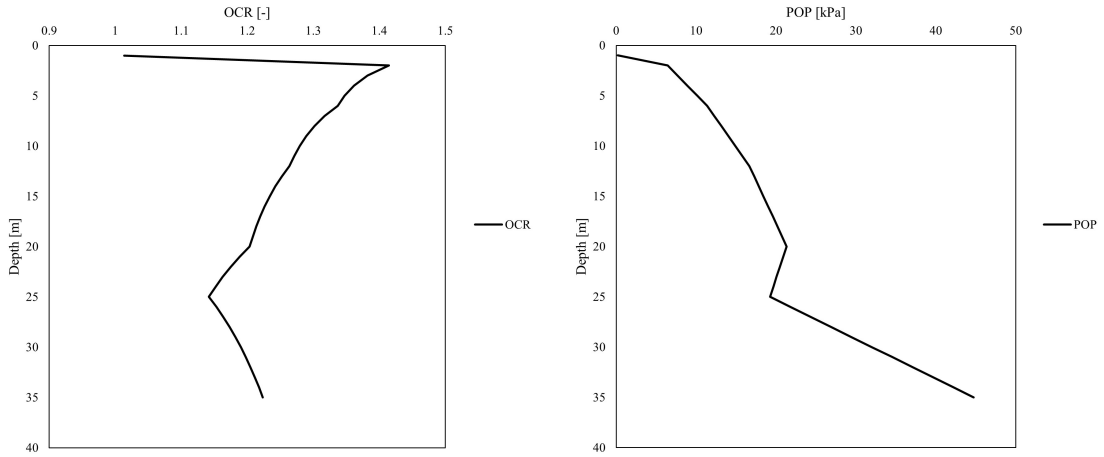

(a) (b)

Figure 3.7: (a) OCR and (b) POP with depth.

The critical state stress ratio, M_c, was calculated according to Equation 3.2 (Knappett & Craig, 2012). The friction angle was put to 30 degrees in accordance with Olsson (2010). Furthermore, the values for absolute rate of destruction, a, and relative effectiveness of destruction, b, were also based on literature. According to Karstunen and Amavasai (2017), a should lay between 8-12 and b should be in the range 0.2-0.4.

$$M_c = \frac{6sin\phi'}{3 - sin\phi'} \tag{3.2}$$

To calculate absolute rate of change of yield surface inclination, μ, effectiveness of yield surface rotation, β, and initial yield surface inclination, α, Equations 3.3-3.5 were used (Karstunen & Amavasai, 2017):

$$\mu \approx \frac{1}{\lambda - \kappa} ln\left(\frac{10M_c^2 + 2\alpha_0\beta}{M_c^2 + 2\alpha_0\beta}\right) \tag{3.3}$$

$$\beta = \frac{3(4M_c^2 - 4\eta_0^2 - 3\eta_0)}{8(\eta_0^2 + 2\eta_0 - M_c^2)} \tag{3.4}$$

$$\alpha_0 = \eta_0 - \frac{M_c^2 - \eta_0^2}{3} \tag{3.5}$$

where η_0 denotes the stress state at the normally consolidated state and was calculated with Equation 3.6:

$$\eta_0 = \frac{3M_c}{6 - M_c} \tag{3.6}$$

The Poisson's ratio was retrieved from Karstunen and Amavasai (2017) who stated that the the parameter should be between 0.1 and 0.2 for soft soil. The hydraulic conductivity was chosen in the range $5 - 10 \cdot 10^{-10}$ meter/second in accordance to Olsson (2010). The coefficient of earth pressure at rest, K_0, was calculated using Jaky's formula. Since the clay was overconsolidated a variant of the equation incorporating the OCR was used, see Equation 3.7 (Swedish Standards Institute, 2005).

$$K_0 = (1 - sin\phi)\sqrt{OCR} \tag{3.7}$$

The final parameters used to model each clay layer are compiled and presented in Table 3.1.

Table 3.1: Input parameters for the clay layers.

Parameter	Layer 1	Layer 2	Layer 3	Layer 4	Layer 5	Layer 6	Unit
Meters below ground surface	0.5-6	6-12	12-20	20-25	25-30	30-35	m
γ_{unsat}	14.6	14.9	15.2	16.2	16.5	16.5	kN/m^3
γ_{sat}	14.6	14.9	15.2	16.2	16.5	16.5	kN/m^3
κ	0.057	0.057	0.05	0.05	0.06	0.065	-
ν'	0.15	0.15	0.15	0.15	0.15	0.15	-
λ	1.00	1.00	1.05	0.97	0.90	0.90	-
M	1.2	1.2	1.2	1.2	1.2	1.2	-
μ	2.07	2.07	1.96	2.13	2.33	2.34	-
β	0.76	0.76	0.76	0.76	0.76	0.76	-
a	10	10	10	10	10	10	-
b	0.3	0.3	0.3	0.3	0.3	0.3	-
OCR	1.31	1.29	1.23	1.16	1.17	1.21	-
POP	-7	-14	-19	-20	-27	-40	kPa
e_0	2.8	2.65	2.3	2.05	1.85	1.6	-
α_0	0.458	0.458	0.458	0.458	0.458	0.458	-
x_0	0	0	0	0	0	0	-
k_x	$6.48 \cdot 10^{-5}$	$6.48 \cdot 10^{-5}$	$6.48 \cdot 10^{-5}$	$6.48 \cdot 10^{-5}$	$6.48 \cdot 10^{-5}$	$6.48 \cdot 10^{-5}$	m/day
k_y	$6.48 \cdot 10^{-5}$	$6.48 \cdot 10^{-5}$	$6.48 \cdot 10^{-5}$	$6.48 \cdot 10^{-5}$	$6.48 \cdot 10^{-5}$	$6.48 \cdot 10^{-5}$	m/day
K_0	0.572	0.567	0.553	0.539	0.541	0.550	-

In Figure 3.1 the constructed test embankment and its dimensions is shown. Additionally, the embankment has a crest length of 25 m. The embankment was modelled using the Mohr-Coulomb model with a drained soil behaviour. The input parameters for the embankment material are presented in Table 3.2. The saturated and unsaturated unit weight as well as the Young's modulus was taken in accordance with those used by Olsson (2010) when modelling the same embankment. Poisson's ratio and the friction angle were taken from one of the benchmark calculations by Vogler (2008) where a similar problem was modelled. As can be seen in Table 3.2, some cohesion was allowed as well to prevent failure of the embankment. The hydraulic conductivity was assumed to be the same in both x- and y-direction. The value of 8.64 meter/day, seen in Table 3.2, was based on the information given by Fetter, C.W. (2001) for well-sorted gravel. The coefficient of earth pressure at rest, K_0, was calculated with Jaky's formula, see Equation 3.8 (Knappett & Craig, 2012).

$$K_0 = 1 - sin(\phi) \tag{3.8}$$

The dry crust was also modelled with a drained soil behaviour using Mohr-Coulomb. The unit weight for the layer was retrieved from a CPT test which was conducted at borehole BH5. The exact location of the borehole is unknown, however it was placed somewhere around the test embankment. It was the only borehole giving information about the dry crust and since the values were reasonable it was chosen for the model. The Poisson's ratio and hydraulic conductivity were assumed to be the same as for the underlying clay. The coefficient of earth pressure at rest was again calculated using Jaky's formula, Equation 3.8. Some cohesion was added to the dry crust as well, to account for suction in the upper soil layer. The assumed input parameters for the dry crust are presented in Table 3.2.

Table 3.2: Input parameters for the embankment and the dry crust.

Parameter	Embankment	Dry crust	Unit
γ_{unsat}	17	16	kN/m^3
γ_{sat}	17	16	kN/m^3
E'	50 000	30 000	kPa
ν'	0.3	0.15	-
c'	6	15	kPa
ϕ'	38	30	degrees
ψ	0	0	degrees
k_x	8.64	$6.48 \cdot 10^{-5}$	m/day
k_y	8.64	$6.48 \cdot 10^{-5}$	m/day
K_0	0.384	0.5	-

3.2 Lime-Cement Column Parameters

The lime-cement columns in Nödinge had a diameter of 0.6 m and were installed in a square pattern, with a column spacing of 1.5 m, where every other column had a length of 12 m and the remaining had a length of 20 m (Alén et al., 2006). The columns were installed in the soil around 7 months before the first embankment layer was constructed and consisted of 50% lime and 50% cement, with a total binder content of 90 kg/m^3 soil.

Although numerous measurements of the soil characteristics are available for the Nödinge site, there is a limited amount of available measurements of the characteristics of the columns. To get an idea of the possible column characteristics in the field and how these compare to guideline values from Trafikverket, results from CAUC triaxial tests on columns presented by NCC for the Westlink project in Gothenburg were analysed (Wood, 2018). However, the features of these tests differ from the conditions in Nödinge, both regarding stress paths and column properties and the results from these tests can therefore not directly be used to determine the characteristics of the lime-cement columns in Nödinge. There were a total of four tests available, two on lime-cement reinforced soil prepared in laboratory and two field samples. The laboratory samples had a larger binder content compared to the Nödinge case, with 110 kg/m^3, and a shorter hardening time of 28 days at 20 $°C$. The column samples taken from the field had smaller binder content, at 50 kg/m^3, the hardening time is however unknown.

In Figure 3.8 the stress-strain curves from the four triaxial tests are presented. The curves differ noticeably from each other, especially between the two field tests. However, the triaxial tests on the field samples had some technical issues which could explain the large difference between the tests and the rather unexpected shape of the curves. These issues included leakage of the confining membrane surrounding the sample, consolidation to a higher stress by mistake and issues with the cell pressure control system. Even though there are differences between the four curves, the reinforced samples, apart from field sample 21, display a considerably higher stiffness compared to the guidelines from Trafikverket. This can for example be seen when comparing the secant shear modulus, G'_{50}, of the reinforced soil samples, presented in Table 3.3, with the G'_{50} given by Trafikverket presented in Table 3.4. These results indicate that the stiffness of the lime-cement columns in Nödinge is likely much higher compared to existing guideline values. Since undrained triaxial tests were performed, the secant elasticity modulus, E_{50}, derived from the stress-strain curves, were converted from an undrained to a drained parameter through Equation 3.9 from Budhu (2010). To obtain the secant shear modulus from the secant elasticity modulus Equation 2.8, presented in section 2.2.2, was used.

$$E' = \frac{E_{undrained}(1 + v')}{1.5} \tag{3.9}$$

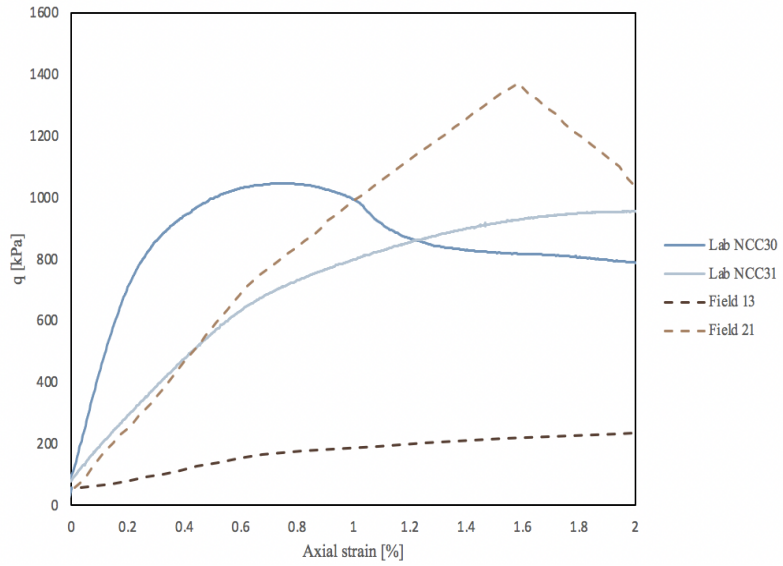

Figure 3.8: Deviatoric stress as a function of axial strain from triaxial tests on lab and field samples of lime-cement reinforced soil.

Table 3.3: Effective secant shear modulus of field and lab samples of lime-cement reinforced soil.

Sample	Secant shear modulus, G'_{50} [kPa]
Lab NCC30	115 952
Lab NCC31	32 444
Field 13	5 370
Field 21	35 136

An attempt to recreate these laboratory results was performed using the Soil test facility in Plaxis. However, it was not possible without using unreasonable values on the parameters inputs.

To investigate how well the use of column guideline values complies with the stress strain response of lime-cement columns measured in field, the Nödinge case was modelled using column guideline values from Trafikverket. In Table 3.4 a full list of the input parameters used in the model is presented. The stiffness of the columns was based on recommendations in TR Geo 13 (Moritz & Karlsson, 2016), presented in Equation 3.10:

$$E_{pel,undrained} = 13{c_{crit}}^{1.6} \tag{3.10}$$

where c_{crit} denotes the critical shear stress, described as the maximum shear stress a lime-cement reinforced soil can hold without developing plastic deformations and can at most be set to 150 kPa. Since the previously described reinforced soil samples were shown to be able to handle shear stresses greater than 150 kPa, c_{crit} was set

to 150 kPa in the model. The elasticity modulus obtained in Equation 3.10 was converted using Equation 3.9 and 2.8, assuming $E_{pel,undrained} = E_{ur,undrained}$.

The cohesion and friction angle of the lime-cement columns were determined based on guideline values in TK Geo 13 (Karlsson & Moritz, 2014). Following these guidelines, the cohesion in the active zone is obtained using Equation 3.11:

$$c = 0.4c_{crit} \tag{3.11}$$

where c_{crit} can be set to 100 kPa as a maximum value for soft columns. Assuming the lime-cement columns are soft and mostly in the active zone, a c_{crit} of 100 kPa was used.

The hydraulic conductivity of the columns were chosen based on Olsson et al. (2008) who stated that this column parameter varied between $0.5 - 5 \cdot 10^{-8}$ m/s in Nödinge. Therefore, a value of $2.75 \cdot 10^{-8}$ m/s was chosen and in similarity with the clay, the hydraulic conductivity was assumed to be the same in both the x- and y-direction. The remaining input parameters for the columns, which are not described in the guidelines from Trafikverket, were assumed based on one of the benchmark calculations by Vogler (2008) where a similar problem was modelled. Additionally, some allowable tensile stress, f_t, was assumed to avoid numerical divergence.

Table 3.4: Input parameters for the lime-cement columns.

Parameter	Value	Unit
c'	40	kPa
ψ	0	Degrees
ϕ'	32	Degrees
G_{ur}^{ref}	12 653	kPa
ν'	0.35	-
m	0.7	-
p'_{ref}	100	kPa
R_f	0.9	-
f_t	5	kPa
G_{50}^{ref}	4 218	kPa
Skempton-B	1	-
k_x	$2.38 \cdot 10^{-3}$	m/day
k_y	$2.38 \cdot 10^{-3}$	m/day

3.3 Additional Parameters in VAT

Additional input parameters related to the VAT model are presented in Table 3.5 below. The column volume ratio, Ω_c, was calculated using Equation 2.12 considering a column diameter of 0.6 m and a column spacing of 1.5 m, following the

column installation in Nödinge (Alén et al., 2006). Since two different lengths of the columns were installed, two values of the volume ratio were calculated to represent the reinforced soil above and below 12 m depth where the shorter columns ended. For the calculation of the Ω_c representing the columns below 12 m depth, half the amount of columns where assumed compared to the Ω_c of the columns above 12 m depth. The Ω_c values presented in Table 3.5 further corresponds to the volume ratios presented by Alén et al. (2006). The parameters *Stepsize* and $init_{strainreduce}$ were assumed based on benchmark calculations by Vogler (2008) on a similar problem.

To determine the hydraulic conductivity of the reinforced soil, an average between the two constituents (soil and columns) was calculated using Equation 3.12. The hydraulic conductivity of the reinforced soil was assumed to be the same in the horizontal and vertical direction ($k_x = k_y$).

$$k_{VAT} = k_{soil}(1 - \Omega_c) + k_{column}\Omega_c \tag{3.12}$$

Table 3.5: Additional input parameters for the VAT model.

Parameter	Value	Unit
Stepsize	0	-
Ω_c above 12 m depth	0.130	-
Ω_c below 12 m depth	0.065	-
$init_{strain,reduce}$	1	-
k_x, k_y above 12 m depth	$3.66{\cdot}10^{-4}$	m/day
k_x, k_y below 12 m depth	$2.16{\cdot}10^{-4}$	m/day

4
Numerical Modelling

The lime-cement reinforced embankment in Nödinge was analysed in Plaxis 2D using a plane strain model with 6-noded triangular elements. The modelled geometry is presented in Figure 4.1, and only half of the embankment was modelled. This was chosen because of the symmetry of the problem. Furthermore, it can be seen that the embankment was divided into two layers. This was due to the embankment being constructed in two phases, first a 1.5 m thick layer followed by a 1.3 m thick layer.

Figure 4.1: Geometry of the problem created in Plaxis 2D.

In Table 4.1 the chosen groundwater flow and deformation boundary conditions applied in Plaxis 2D are presented. The X_{min} flow boundary was put as *Closed* due to the line of symmetry. Further, Y_{min}, Y_{max} and X_{max} were put as *Open*. The reasoning behind Y_{min} being open was the more permeable friction soil layer upon the bedrock. Therefore it was assumed that water could be drained in this direction. Furthermore, it was assumed that there was no movement in the horizontal direction at the X_{min} and X_{max} boundary, hence the deformation boundary was put to *Normally fixed*. The Y_{min} boundary was assumed to be *Fully fixed* due to the underlying bedrock. Finally, Y_{max} was assumed to be *Free*.

Table 4.1: Groundwater flow and deformation boundary conditions.

Boundary	Groundwater flow Conditions	Deformation Conditions
X_{min}	Closed	Normally fixed
X_{max}	Closed	Normally fixed
Y_{min}	Open	Fully fixed
Y_{max}	Open	Free

The construction phases used in the analysis are presented in Table 4.2. The initial stress state was generated using the K_0-procedure, which was considered to be a suitable option due to the horizontal soil layers and ground surface. An additional initialisation phase was added to account for the initialisation of the state variables used in the VAT model. Furthermore it should be noted that in many cases the embankment had to be divided into multiple thinner layers for the calculation to run successfully. The same goes for the consolidation phases, which were divided into phases with shorter duration.

Table 4.2: Construction phases and consolidation times.

Construction phase	Type of analysis
Initial phase	K_0 procedure
Initialisation	Plastic
Installing lime-cement columns	Plastic
Construction of 1.5 m embankment, 1 day	Consolidation
Consolidation, 658 days	Consolidation
Construction of 1.3 m embankment, 1 day	Consolidation
Consolidation, 1482 days	Consolidation

To determine a suitable mesh, a mesh sensitivity analysis was conducted. The final mesh used in the analysis is presented in Appendix B as well as the result of the mesh sensitivity analysis. The mesh was gradually refined to ensure convergence of the result, starting from a medium mesh and further refining the embankment, dry crust and lime-cement reinforced soil layers.

4.1 Analyses

As mentioned in Section 3.2, the lime-cement column material tested in laboratory displayed a very high stiffness, suggesting that the stiffness of the lime-cement columns in Nödinge is considerably higher compared to guideline values from Trafikverket. To investigate what effect an increased column stiffness has on the stress-strain response of the reinforced soil and how this compare to settlement measurements made in the field, several analyses with increasing column stiffness were conducted. In Table 4.3 the input values of the column stiffness parameters G_{ur}^{ref} and G_{50}^{ref} for the different analyses are presented. The stiffness was increased by multiplying the Trafikverket guideline values by 2, 5, 10, 15 and 20 respectively. This means that

the increase was within limits to what was measured in the laboratory, presented in Table 3.3 previously. As can be seen in Table 4.3, the allowable tensile stress, f_t, was slightly increased to avoid numerical divergence.

Table 4.3: Deviations from before given input for different models.

Analysis	G_{ur}^{ref} [kPa]	G_{50}^{ref} [kPa]	f_t [kPa]
Trafikverket original	12 653	4 218	5
Trafikverket Gx2	25 310	8 436	8
Trafikverket Gx5	63 265	21 088	8
Trafikverket Gx10	126 530	42 177	10
Trafikverket Gx15	189 795	63 265	12
Trafikverket Gx20	253 060	84 353	12

It became evident that the model did not fully capture the soil behaviour measured in field, described further in Chapter 5. Since the hydraulic conductivity was chosen from a range, it was decided to modify these values, through an iterative process, to see if it was possible to better match the soil's behaviour. New input is presented in Appendix C.

4.1.1 Sensitivity Analysis

A sensitivity analysis was conducted for the soil parameters κ, λ and POP. To limit the number of simulations performed, the value of the column stiffness and hydraulic conductivity was kept constant, using the *Trafikverket Gx5 k3* file for all sensitivity analyses. The *Trafikverket Gx5 k3* file corresponds to the column stiffness and hydraulic conductivity best capturing the soil behaviour measured at the Nödinge site. κ and λ were included in the sensitivity analysis due to the scatter seen in the result from the CRS tests, shown previously in Figure 3.6. To cover most of the scatter, the κ and λ values were increased and decreased by 0.01 and 0.1 respectively. The values of μ was also recalculated due to its dependency on κ and λ and these values are presented in Appendix D together with the chosen values of κ, λ and POP. Additionally, the POP was varied as if the groundwater table varied $\pm$ 0.5 m. Due to time restraints, the geometry and level of the water table in the Plaxis model was kept unchanged.

5
Results

The vertical displacement for increasing column stiffnesses is presented in Figure 5.1 below. The available vertical displacement measured at site, presented in black in the figure, were retrieved at 2 m depth, hence all modelled vertical displacements were retrieved at the same depth. In the figure it can be seen that the vertical displacement, using a column stiffness corresponding to the guideline values from Trafikverket (denoted as Trafikverket original), is noticeably larger compared to the vertical displacement measured at the site in Nödinge. As expected, an increased column stiffness results in lower vertical displacements, with a final settlement of roughly 22 cm for a stiffness 20 times larger than the Trafikverket guidelines compared to 36 cm for the original Trafikverket guideline stiffness. Furthermore, the stiffness 20 times larger than the guidelines results in the lowest final settlement, only 4 centimeters from the measured final settlements at the Nödinge site. However, the effect of the column stiffness on the deformation behaviour of the reinforced system seems to lessen with increasing stiffness. This is visualised in Figure 5.1, where the difference in vertical displacements between Gx2 and Gx5 is much larger compared to Gx15 and Gx20.

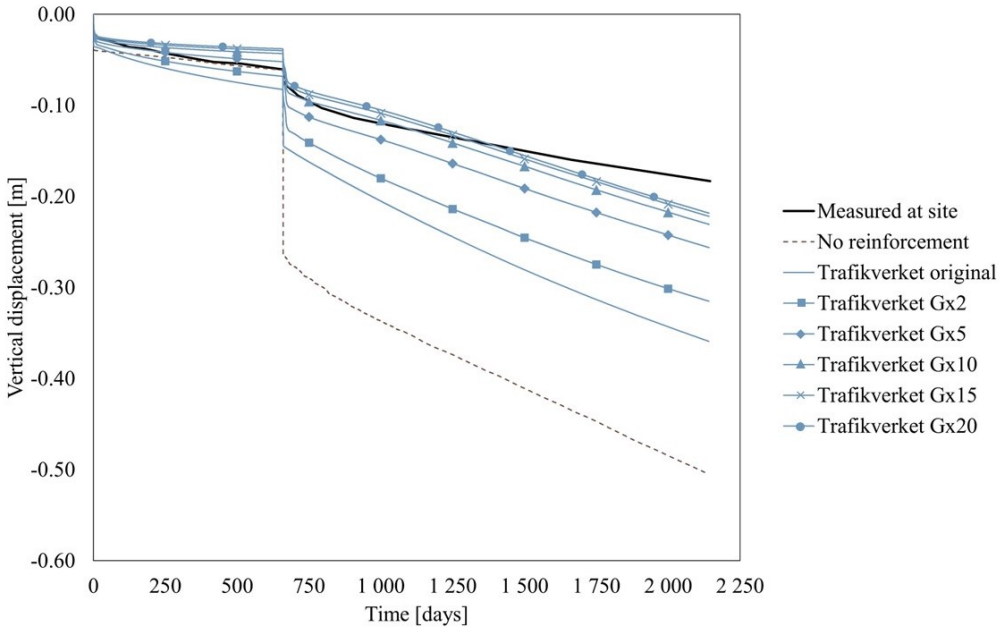

Figure 5.1: Vertical displacement, at the centerline of the embankment and at 2 m depth, over time using different shear modulus for the columns.

While the increased stiffness of the columns generate a final settlement corresponding better with the settlements measured at the site, it can be seen that the modelled settlements do not fully capture the real behaviour of the soil. As can be seen in Figure 5.1, the settlement rate at the second consolidation period is visibly higher for each of the simulations compared to the measured settlement rate. These results could be because of the presence of less permeable layers at the site, which are not included in the model, or a too high hydraulic conductivity being used in the model. Since the hydraulic conductivity for both the columns and the soil is taken from a range, it is possible that the values used in the model are too high. Therefore, the hydraulic conductivity was reduced gradually, within the ranges presented in Section 3.1 and 3.2, until a better fit with the measured data was achieved. In Figure 5.2 the vertical displacement using lower hydraulic conductivities is presented. It can be seen that a good fit was found with the analysis *Trafikverket Gx5 k3*, see Appendix C for the corresponding hydraulic conductivity.

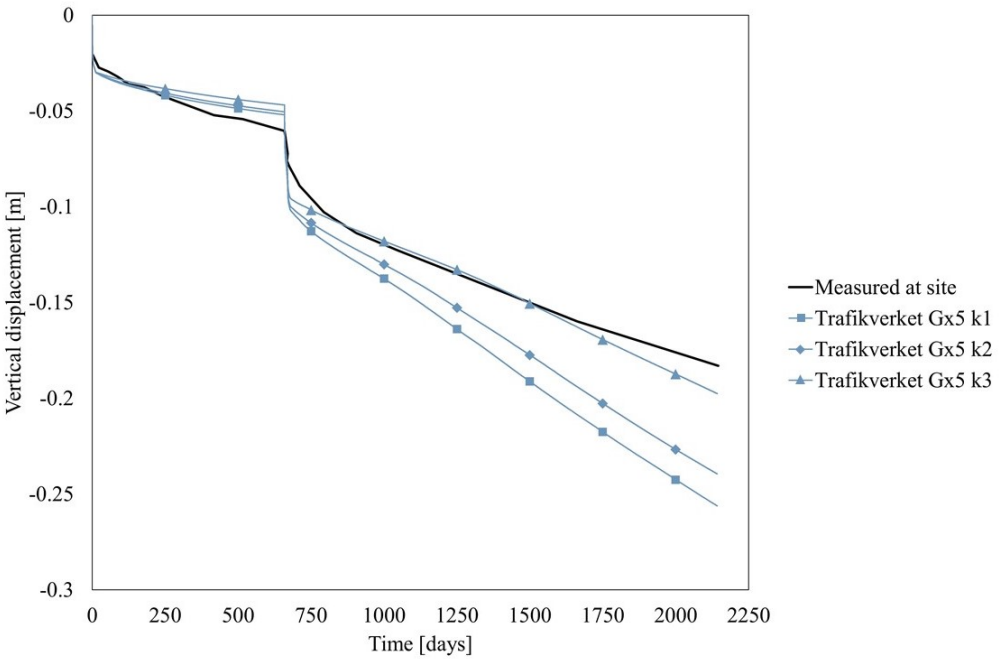

Figure 5.2: Vertical displacement, at the centerline of the embankment and at 2 m depth, using different values of hydraulic conductivity.

In Figure 5.3 the vertical displacement for different column stiffnesses is displayed, where the hydraulic conductivity has been modified to better capture the behaviour of the soil. For a column stiffness corresponding to the guidelines from Trafikverket the settlements reached 29 cm after 2142 days. For the column stiffness Gx5, the settlements are 19 cm after the same time period, which is only 1.5 cm larger than those measured at the site. Similar to the result presented in Figure 5.1, the vertical displacements reduce with the increase in column stiffness. However, compared to the previous result, two main differences can be identified. The first being that the behaviour of the soil has been better captured by the model and second one being that the settlements are lower for all stiffnesses. Due to this, the stiffness only had

to be increased to 5 times the original size to reach similar settlements as measured at the site.

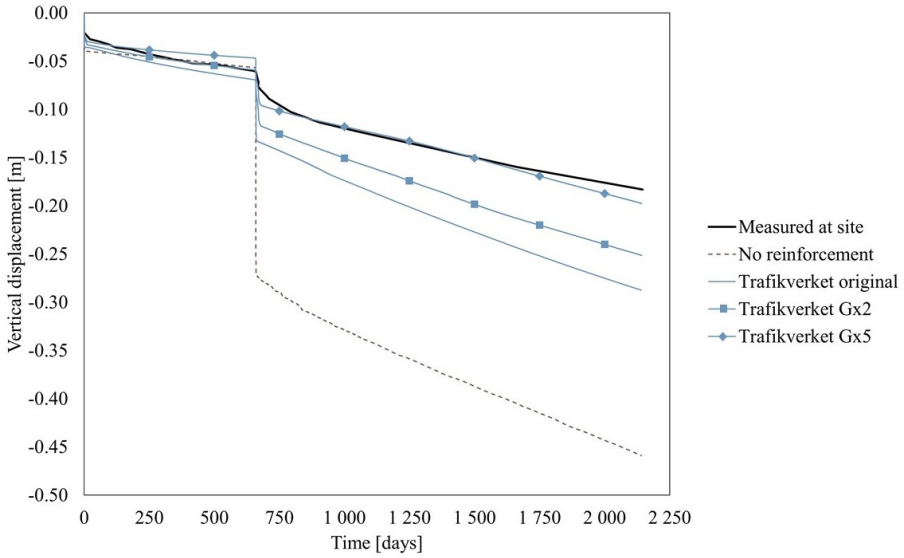

Figure 5.3: Vertical displacement, at the centerline of the embankment and at 2 m depth, over time using different shear modulus for the columns. With modified hydraulic conductivity to better capture the behaviour of the soil.

As presented in Section 3.2 and Figure 3.8, the lime-cement reinforced soil samples tested in laboratory generally showed a very high stiffness compared to the guidelines from Trafikverket. Therefore the stress-strain relationship of the modelled lime-cement columns were analysed using the soil test facility in Plaxis. These results are presented in Appendix E, and as can be seen a convergence between the modelled stress-strain relationship and the one analysed in laboratory was not achieved. This type of divergence is not in the scope of the thesis, hence it is not investigated further.

In addition to vertical displacements, the horizontal displacement under the embankment (6.5 m from the centerline) was analysed for different values of the column stiffness, see Figure 5.4. As visible in the figure, an increase in column stiffness results in reduced horizontal displacements, where the lowest displacements are seen for the stiffness 5 times larger than the stiffness guidelines from Trafikverket. A somewhat unexpected result is seen in the dry crust. This is probably due to the partial improvement of the dry crust's stiffness, as a result of the lime-cement columns, not being considered.

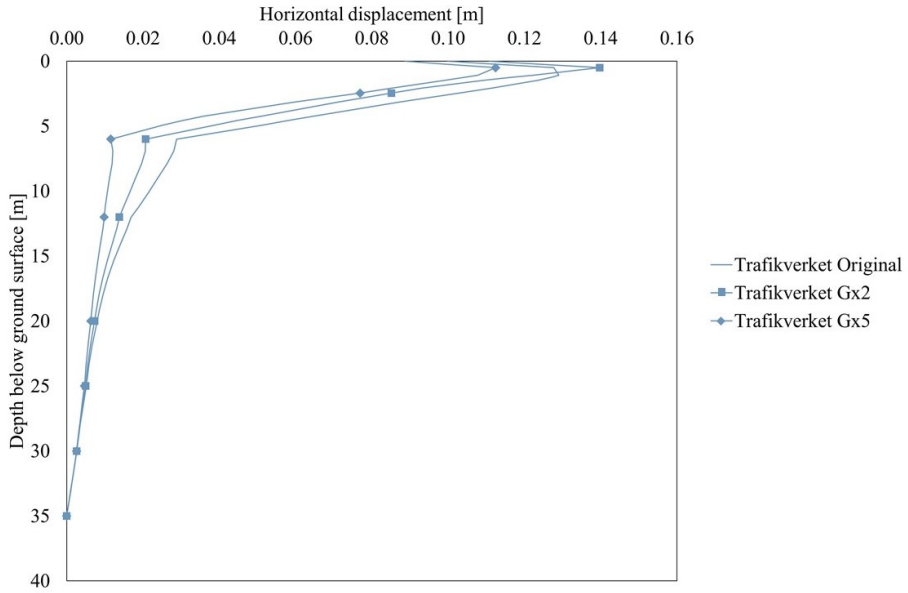

Figure 5.4: Measured horizontal displacement under the embankment (6.5 m from the centerline) using different column stiffness.

Finally, the result of the conducted sensitivity analysis is presented in Figures 5.5-5.7. It can be seen that the model is slightly sensitive to lower values of κ, however only small result differences can be observed. For higher κ values the result is less sensitive. In Figure 5.6 it is clearly visible that the model is not sensitive to the choice of λ value. However, the sensitivity analysis for POP shows a high model sensitivity. The result clearly shows the importance of having a knowledge of the location of the groundwater level since it highly affects the POP. Note that the geometry and groundwater level was not changed in the model for the sensitivity analysis due to time constraints.

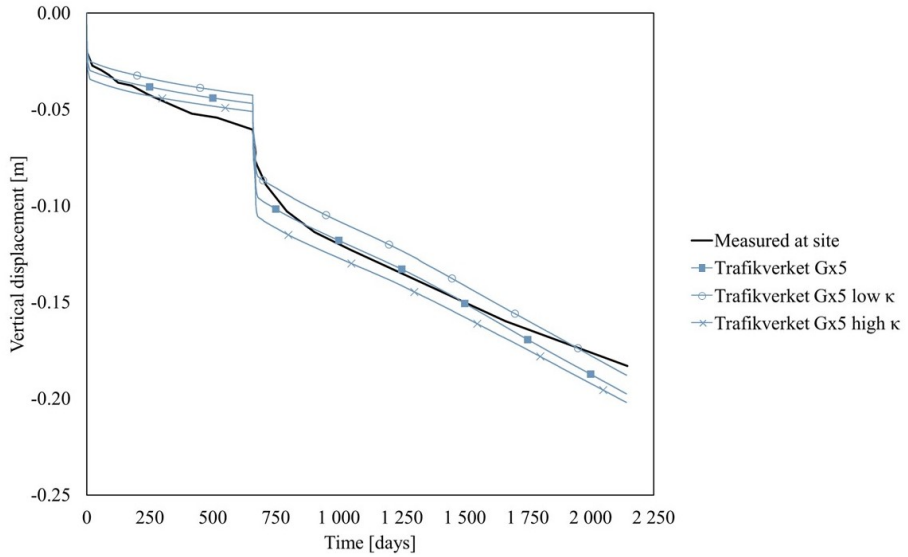

Figure 5.5: Vertical displacement, at the centerline of the embankment and at 2 m depth, using different values of κ.

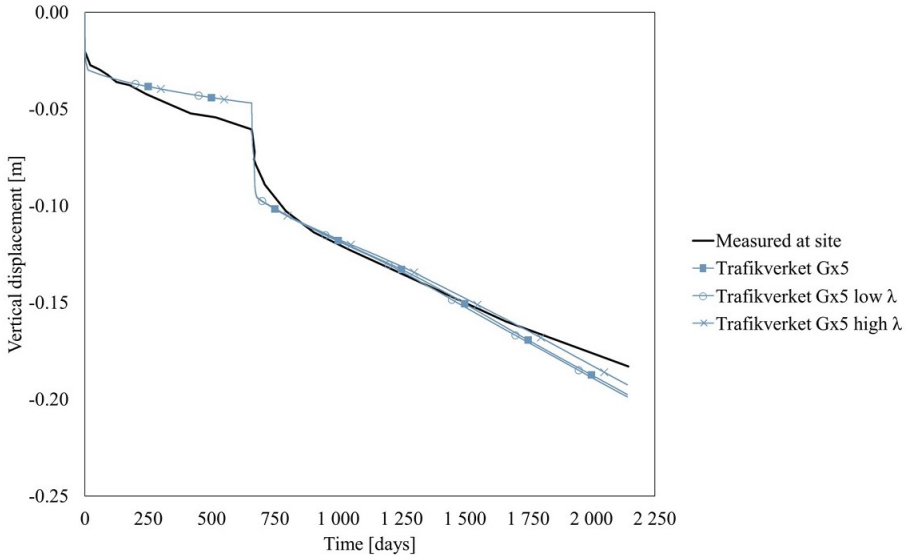

Figure 5.6: Vertical displacement, at the centerline of the embankment and at 2 m depth, using different values of λ.

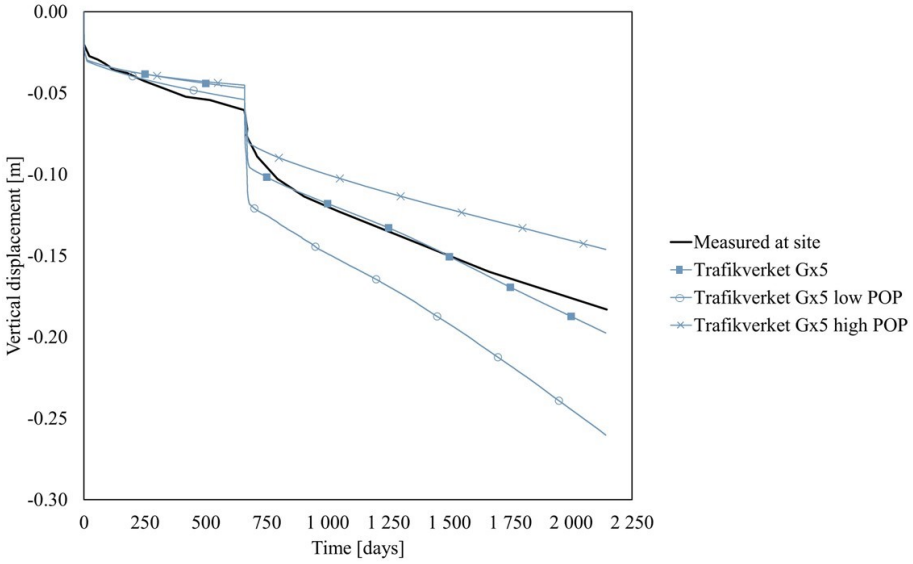

Figure 5.7: Vertical displacement, at the centerline of the embankment and at 2 m depth, using different values of POP.

6
Discussion

As presented in Chapter 5, using a column stiffness corresponding to the Trafikverket guidelines in TR Geo 13 results in larger settlements than those measured at the Nödinge site. This is for example visible in Figure 5.3, where the settlement using Trafikverket's stiffness guidelines is 10 cm larger. It was further observed that when increasing the column stiffness the settlements decreased and approached the at site measured settlements, indicating that the actual stiffness of the columns in Nödinge is considerably higher than Trafikverket's guideline values. In fact, a stiffness 5 times larger than the guideline value is needed to reach the settlements measured at the site. However, as previously presented the soil samples was of varying quality. Therefore it is important to keep in mind that the need of a higher column stiffness could have been affected by the soil parameters being inaccurate.

The use of an increased column stiffness is supported by the results from triaxial tests on lime-cement columns from both field and laboratory, see Section 3.2. These results displayed an effective secant shear modulus in the range of 5 370 - 115 952 kPa compared to a value of 4 218 kPa proposed by Trafikverket. Furthermore, two of the column samples, Lab NCC31 and Field 21, displayed a stiffness relatively close to the Gx5 stiffness, which as can be seen in Figure 5.3 corresponds to a settlement closest to the one measured in Nödinge. However, the lowest value of the range is fairly close to the Trafikverket guideline. Additionally, there is a considerable difference between the highest and the lowest value of the range. This indicates that further testing on lime-cement reinforced samples is needed to be able to draw a well supported conclusion regarding the Trafikverket guidelines with respect to column stiffness.

The large difference in column stiffness, seen from the triaxial tests on lime-cement reinforced soil samples, could partly be due to the differences between field and laboratory samples previously presented in Section 3.2. The samples differed both regarding the amount of binder and the hardening time, as well as the fact that the samples were prepared either in field or directly in the laboratory. Furthermore, there were several issues related to the reinforced samples prepared in the field, for example regarding the cell pressure control system and the confining membrane surrounding the sample, which further most likely contributed to the variation in stiffness. Another possible contributing factor to the differences in stiffness between samples is the fact that the final stabilisation effect of a reinforced soil is influenced by the type of soil and the mixing process, described in Section 2.1. These factors will consistently be involved in the lime-cement column installation, and uncertain-

ties regarding the stiffness of the columns therefore need to be considered when designing the columns. Both the soil type and the mixing process affect the homogeneity of the column. The differences in soil type is difficult to overcome, however the mixing process is easier to adjust. Therefore, it is suggested that the mixing process is studied further to possibly improve the homogeneity of lime-cement columns.

The variation in stiffness between different samples of reinforced soil, shown in Section 3.2, has also been seen by Ignat (2015). In the study, isotropic undrained triaxial tests were performed on lime-cement reinforced clay samples. The samples generally displayed slightly lower stiffnesses compared to the samples presented in this thesis, with a corresponding effective secant shear modulus of between 4 000 - 26 000 kPa. In comparison with the stiffness guideline from Trafikverket, the lowest value in the range is very similar to the guideline while the highest value of 26 000 kPa is close to 5 times the size of the guideline, indicating the large difference in column stiffness between reinforced soil samples.

In the guidelines proposed by Trafikverket in TR Geo 13 (Moritz & Karlsson, 2016) a maximum critical shear stress, c_{crit}, of 150 kPa is advised for the calculation of the column stiffness. When considering the resulting stress-strain curves from the triaxial tests on lime-cement columns, presented in Section 3.2, higher values of c_{crit} can be seen for the laboratory samples, NCC30 and NCC31. The two column samples display a c_{crit} of around 700 kPa (calculated as 70% of the failure load), a significantly higher value compared to the critical shear stress in TR GEO 13. For the two field samples, test 13 and 21, the critical shear stress is less consistent between the two tests. As previously discussed, there were several issues during the laboratory tests resulting in less reliable results.

Even though there are uncertainties regarding the column stiffness, as previously discussed, the achieved result shows a possible tendency of the stiffness guidelines given by Trafikverket being too low. A consequence of having too low guidelines, which are not fully based on reality, is the need for a higher number of columns or larger column dimensions. Such an excessive design could lead to higher costs as well as a greater environmental impact. For lime-cement columns the cement contributes with the largest environmental impact, as cement stands for around 8% of the worlds CO_2-emissions (Ellis et al., 2020). Therefore it is of high interest to use cement to a minimum, while still obtaining the required strength and stability.

Further in connection to the column stiffness, it can be seen in Figure 5.1 that using a column stiffness 10 times larger than Trafikverket's guideline value results in roughly the same settlements as when using a columns stiffness 20 times larger. According to Åhnberg et al. (1995) the column stiffness increases with an increased binder content. Thereby, in terms of settlements, the obtained results suggest that a lower binder content could be used without significantly affecting the performance of the columns. However, the column stiffness seems to have a greater impact on the column performance for stiffness values in the lower range. From one of the obtained lab results, NCC30, the column stiffness was around 120 000 kPa, indicating

that in reality lime-cement columns have a stiffness as large as 20 times the stiffness guidelines from Trafikverket. Therefore, it is of interest to further investigate the impact of column stiffness on the deformation behaviour and its connection to binder content. This is of interest especially to investigate the possibility of reducing the binder content in order to minimise the environmental impact of lime-cement columns previously discussed.

The achieved results indicate that the model is mainly sensitive to the choice of input data for the columns and less sensitive to the soil data. This is visible from the sensitivity analysis where the model shows a slight sensitivity to the choice of both κ and λ. It should however be kept in mind that the changes made for the value of κ were relatively small and it is likely that larger changes would lead to greater result differences, especially if a lower κ value is used. Olsson (2010) suggests the use of lower κ values since the stiffness in the overconsolidated regions is often underestimated in laboratory. The reason for this underestimation might be sample disturbance and the sample reconsolidation process in laboratory. To better model the real stiffness of the soil it is therefore suggested that the value of κ could be lowered. Based on the received result a lower κ would lead to less settlements, hence the installed columns might have a lower stiffness than what the conducted analyses suggest.

Even though the model is less sensitive to the changes in soil parameters, a noticeable sensitivity can be seen for the POP value, as can be seen in Figure 5.7. This suggests that the model is sensitive to the location of the groundwater table. As mentioned before, the location of the groundwater table was not changed in the model when conducting the POP sensitivity analysis. If it would have been changed in accordance to the chosen POP values it is possible that the result would diverge even more. Another example of the importance of input parameters was seen for the hydraulic conductivity. The settlement rate is highly dependent on the hydraulic conductivity and small differences will have larger impacts on the final settlement. With regards to these examples and what has been discussed previously, special attention needs to be payed to the input parameters to be able to optimise the system and achieve satisfactory results regarding settlements, costs and environmental impact.

7
Conclusion

In this thesis, a test embankment in Nödinge, reinforced with lime-cement columns, was studied using the Volume Averaging Technique in Plaxis 2D. The Volume Averaging Technique implements two individual constituents, soil and column, modelling them as a composite material, simplifying a three-dimensional problem into a two-dimensional problem. The purpose of this work was to study the impact of lime-cement column characteristics on the stress-strain response of the system in Nödinge. Comparisons were made between the at site measured settlements and those modelled using Plaxis 2D. Furthermore, it was studied how well the guidelines from Trafikverket corresponded with the modelled and measured deformation behaviour.

In conclusion, the settlement using a column stiffness corresponding to guidelines in TR Geo 13 from Trafikverket reached 29 cm. This is 10 cm more compared to the settlements measured at the Nödinge site. It has been proven that the settlements reduces with an increased column stiffness. With a stiffness 5 times larger than that given by the guideline, the settlements are only 1.5 cm larger than those measured at the site.

The simulations suggest that the column stiffness used in field is much larger than those given in the guidelines from Trafikverket. This is partly supported by the laboratory results which overall showed a higher stiffness than that of the guidelines. However, the results also show a large span of stiffnesses, from values close to the guidelines to those twenty times larger. This suggests that lower values may be necessary to account for the uncertainties connected to the column stiffness in order to minimise the risk of designing a system with poor functionality. The uncertainties regarding the homogeneity of the columns also suggests that lower guideline values are needed to account for the possible occurrence of weaker layers in the columns. Since cement is such a large contributor to the world's CO_2-emissions it is of high interest to lower the use of cement. Therefore, further investigations on how well the guidelines coincides with the actual stiffness of lime-cement columns used in field, are suggested. In addition, the relation between column stiffness and factors such as binder content, mixing procedure and soil type needs to be investigated further.

Bibliography

Abed, A., Vogler, U., & Karstunen, M. (Submitted). Volume Averaging Technique for modelling of deep mixed columns: theory, implementation, and numerical application. *Computers and Geotechnics*.

Åhnberg, H., Johansson, S. E., Retelius, A., Ljungkrantz, C., Holmqvist, L., & Holm, G. (1995). *Cement och kalk för djupstabilisering av jord*. Statens Geotekniska Institut. Linköping.

Alén, C., Sällfors, G., Bengtsson, E., & Baker, S. (2006). *Provbankar Riksväg 45/Nordlänken Bankar på kalkcementpelarförstärkt jord-Beräkningsmodell för sättningar*. Swedish Deep Stabilization Research Centre. Linköping. www.swedgeo.se/sd.

Baker, S., Sällfors, G., & Alén, C. (2005). Deformation properties of lime/cement columns. Evaluation from in-situ full scale tests of stabilised clay. *Deep Mixing '05*.

Becker, P., & Karstunen, M. (2013). Volume averaging technique in numerical modelling of floating deep mixed columns in soft soils. *Installation Effects in Geotechnical Engineering - Proceedings of the International Conference on Installation Effects in Geotechnical Engineering, ICIEGE 2013*.

Benz, T., Wehnert, M., & Vermeer, P. A. (2008). *A Lode Angle Dependent Formulation of the Hardening Soil Model*.

Benz, T. (2007). *Small-strain stiffness of soils and its numerical consequences* (Doctoral dissertation).

Bower, T. A., Jefferson, A. D., & Cleall, P. J. (2020). A reformulated hardening soil model. *Proceedings of the Institution of Civil Engineers: Engineering and Computational Mechanics*, *173*(1), 11–29. https://doi.org/10.1680/jencm.18.00054

Brinkgreve, R., & Vermeer, P. A. (2021). *PLAXIS 2D-Reference Manual V22*. Delft. https://communities.bentley.com/products/geotech-analysis/w/plaxis-soilvision-wiki/46137/manuals---plaxis

Budhu, M. (2010). *Soil Mechanics and Foundations, 3rd Edition*. John Wiley & Sons, Incorporated.

Carlsten, P. (1996). Chapter 10 Lime and lime/cement columns. *Developments in geotechnical engineering*. https://doi.org/10.1016/S0165-1250(96)80013-7

Carlsten, P. (2000). *Kalk- och kalkcementpelare*. Swedish Geotechnical Society. Linköping.

Danas, K., Castañeda, P. P., Danas, K., & Ponte Castañeda, P. (2012). *Influence of the Lode parameter and the stress triaxiality on the failure of elasto-plastic porous materials elasto-plastic porous materials*. https://hal-polytechnique.archives-ouvertes.fr/hal-00755852

Ellis, L. D., Badel, A. F., Chiang, M. L., Park, R. J.-Y., & Chiang, Y.-M. (2020). Toward electrochemical synthesis of cement—An electrolyzer-based process for decarbonating $CaCO_3$ while producing useful gas streams. *Proceedings of the National Academy of Sciences*, *117*(23), 12584–12591. https://doi.org/10.1073/pnas.1821673116

EN 14679. (2005). *Execution of special geotechnical works-Deep mixing*. www.sis.se

Fetter, C.W. (2001). *Applied Hydrogeology* (Fourth edition). Pearson.

Forsberg, T. (2021). *Järnväg för höghastighetståg – alternativa grundläggningsmetoder vid hårda sättningskrav*. Trafikverket.

Gao, Z., Zhao, J., & Yao, Y. (2010). A generalized anisotropic failure criterion for geomaterials. *International Journal of Solids and Structures*, *47*(22-23), 3166–3185. https://doi.org/10.1016/j.ijsolstr.2010.07.016

Gens, A., & Nova, R. (1993). Conceptual bases for a constitutive model for bonded soils and weak rocks. *Proceedings of the Second International Symposium on Hard Soils-Soft Rocks*.

Google. (2022). Google Maps. https://goo.gl/maps/ai1SLjKrcGAHhYuf7

Graham, J., Noonan, M. L., & Lew, K. V. (1983). Yield states and stress–strain relationships in a natural plastic clay. *Canadian Geotechnical Journal*, *20*(3), 502–516. https://doi.org/10.1139/t83-058

Ignat, R. (2015). *Field and Laboratory Tests of Laterally Loaded Rows of Lime-Cement Columns* (Doctoral dissertation). Royal institute of Technology. Stockholm.

Karlsson, M., & Moritz, L. (2014). Trafikverkets tekniska krav för geokonstruktioner TK Geo 13.

Karstunen, M., Wiltafsky, C., Krenn, H., Scharinger, F., & Schweiger, H. F. (2006). Modelling the behaviour of an embankment on soft clay with different constitutive models. *International Journal for Numerical and Analytical Methods in Geomechanics*, *30*(10), 953–982. https://doi.org/10.1002/nag.507

Karstunen, M., & Amavasai, A. (2017). *BEST SOIL: Soft soil modelling and parameter determination*.

Karstunen, M., & Koskinen, M. (2008). Plastic anisotropy of soft reconstituted clays. *Canadian Geotechnical Journal*, *45*(3), 314–328. https://doi.org/10.1139/T07-073

Karstunen, M., Krenn, H., Simon, ; Wheeler, J., Koskinen, M., & Zentar, R. (2005). Effect of Anisotropy and Destructuration on the Behavior of Murro Test Embankment. *International Journal of Geomechanics*, *5*(2), 87–97. https://doi.org/10.1061/ASCE1532-364120055:287

Knappett, J., & Craig, R. (2012). *Craig's Soil Mechanics* (8th ed.). Spoon Press.

Koskinen, M., Karstunen, M., & Wheeler, S. (2002). Modelling destructuration and anisotropy of a natural soft clay. In P. Mestat (Ed.), *Numerical methods in geotechnical engineering*. Presses de l'ENPC/LCPC.

Labuz, J. F., & Zang, A. (2012). Mohr-Coulomb failure criterion. *Rock Mechanics and Rock Engineering*, *45*(6), 975–979. https://doi.org/10.1007/s00603-012-0281-7

Larsson, R. (2006). *Rapport 17 Djupstabilisering med bindemedels-stabiliserade pelare och masstabilisering-En vägledning*. Svensk Djupstabilisering. www.swedgeo.se.

Larsson, R., Sällfors, G., Eriksson, L., Bengtsson, P.-E., Alén, C., & Bergdahl, U. (2007). *Skjuvhållfasthet - utvärdering i kohesionsjord*. Statens geotekniska institut. Linköping. https://www.swedgeo.se/globalassets/publikationer/info/pdf/sgi-i3.pdf

Lee, J. S., & Pande, G. N. (1998). Analysis of Stone-Column Reinforced Foundations. *International Journal for Numerical and Analytical Methods in Geomechanics*, *22*, 1001–1020.

Mohsan, M., Vardon, P. J., & Vossepoel, F. C. (2021). On the use of different constitutive models in data assimilation for slope stability. *Computers and Geotechnics*, *138*. https://doi.org/10.1016/j.compgeo.2021.104332

Moritz, L., & Karlsson, M. (2016). Trafikverkets tekniska råd för geokonstruktioner-TR Geo 13.

Olsson, M. (2010). *Calculating long-term settlement in soft clays-with special focus on the Gothenburg region*. Swedish Geotechnical Institute. Linköping. www.swedgeo.se

Olsson, M., Edstam, T., & Alén, C. (2008). Some experiences from full-scale test embankments on floating lime-cement columns. In M. Karstunen & M. Leoni (Eds.), *Geotechnics of soft soils: Focus on ground improvement* (1st ed.). CRC Press.

Roscoe, K., & Burland, J. (1968). On the Generalized Stress-Strain Behavior of Wet Clays. In J. Heyman & F. Leckie (Eds.), *Engineering plasticity*. Cambridge University Press.

Sivasithamparam, N., Karstunen, M., & Bonnier, P. (2015). Modelling creep behaviour of anisotropic soft soils. *Computers and Geotechnics*, *69*, 46–57. https://doi.org/10.1016/j.compgeo.2015.04.015

Statens Geotekniska Institut. (2009). *Linköping 2012 Slutrapport Del 2-Kartläggning*. www.swedgeo.se

Swedish Standards Institute. (2005). *Eurokod 7: Dimensionering av geokonstruktioner-Del 1: Allmänna regler Eurocode 7: Geotechnical design-Part 1: General rules*. www.eurokoder.se,

Topolnicki, M. (2016). *General overview and advances in Deep Soil Mixing*. https://www.researchgate.net/publication/337801273

Vogler, U., & Karstunen, M. (2009). Application of volume averaging technique in numerical modelling of deep mixing. *Geotechnics of Soft Soils - Focus on Ground Improvement - Proceedings of the 2nd International Workshop on Geotechnics of Soft Soils*. https://doi.org/10.1201/9780203883334.ch22

Vogler, U. (2008). *Numerical Modelling of Deep Mixing with Volume Averaging Technique* (Doctoral dissertation).

Wheeler, S. (1997). A rotational hardening elasto-plastic model for clays. *14th International Conference on Soil Mechanics and Foundation Engineering*.

Wood, T. (2018). *Fullskaleförsök DDM (Dry Deep Mixing) i passivzon, delprojekt E02 Centralen, Västlänken.* Trafikverket.

Xiang, X., & Zi-Hang, D. (2017). Numerical implementation of a modified Mohr–Coulomb model and its application in slope stability analysis. *Journal of Modern Transportation*, *25*(1), 40–51. https://doi.org/10.1007/s40534-017-0123-0

Yu, M. H. (2002). Advances in strength theories for materials under complex stress state in the 20th century. https://doi.org/10.1115/1.1472455

A

Calibration of CRS-Curves

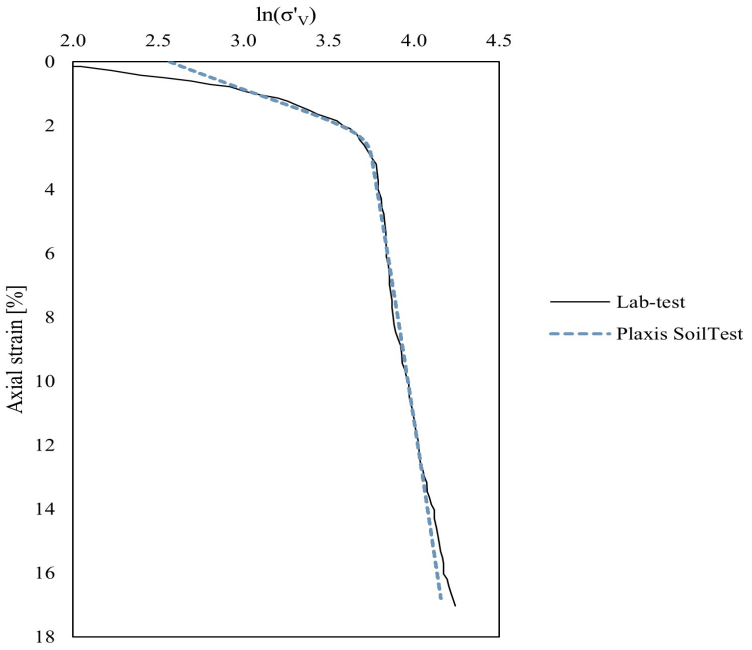

Figure A.1: Calibration of curves from Lab-test and Plaxis SoilTest at 4m depth, BH10010.

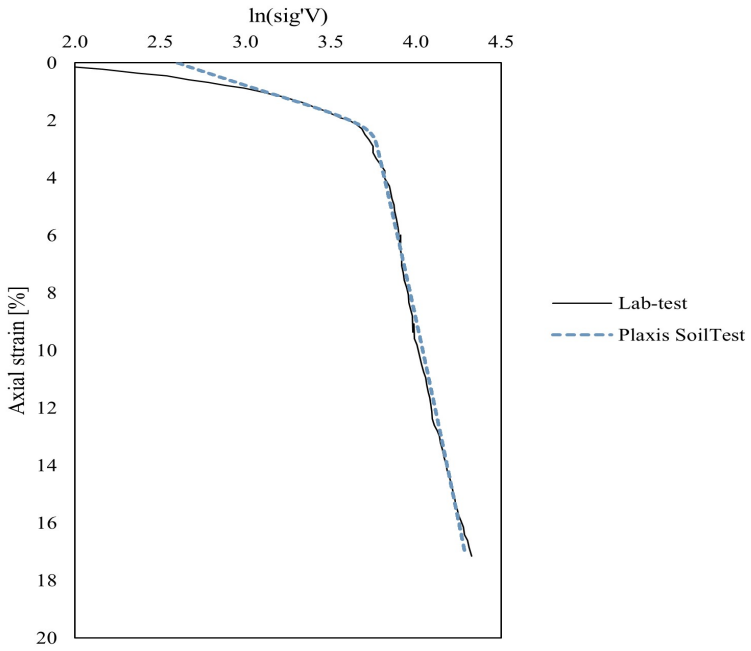

Figure A.2: Calibration of curves from Lab-test and Plaxis SoilTest at 6m depth, BH10010.

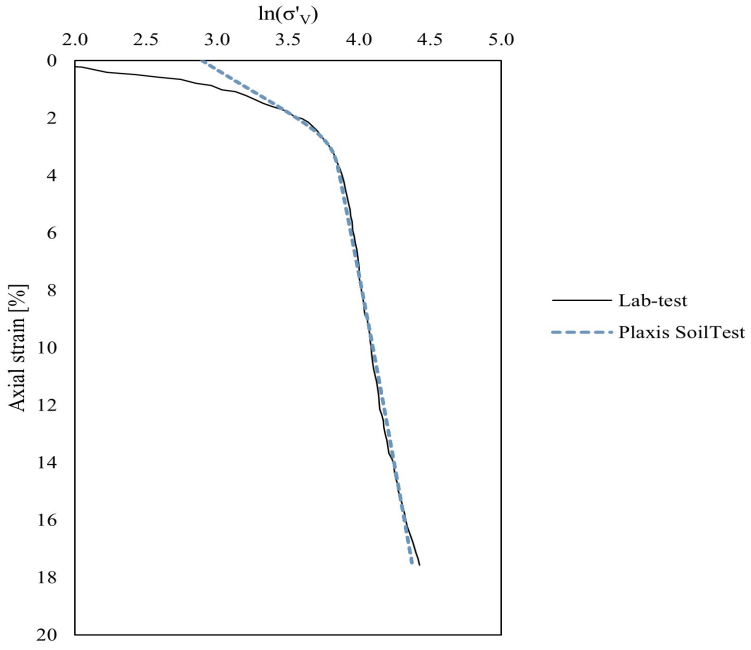

Figure A.3: Calibration of curves from Lab-test and Plaxis SoilTest at 8m depth, BH10010.

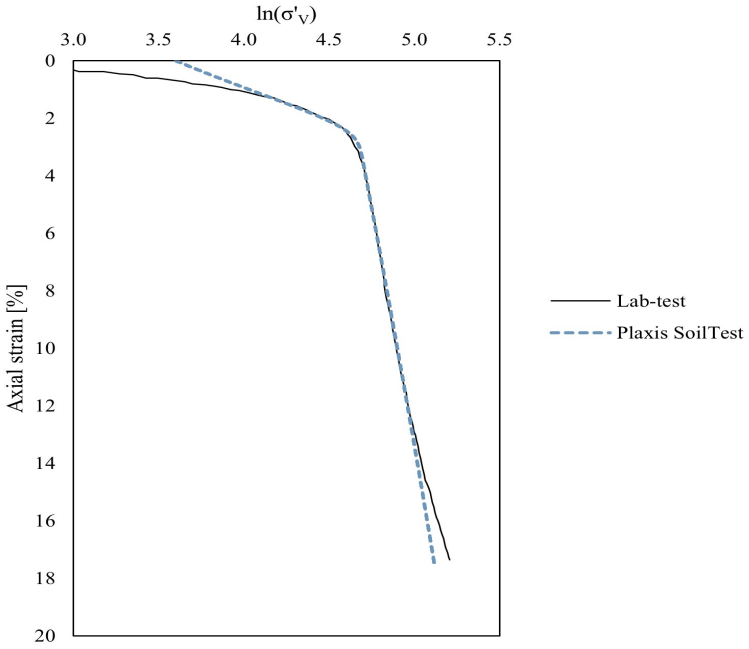

Figure A.4: Calibration of curves from Lab-test and Plaxis SoilTest at 15m depth, BH10010.

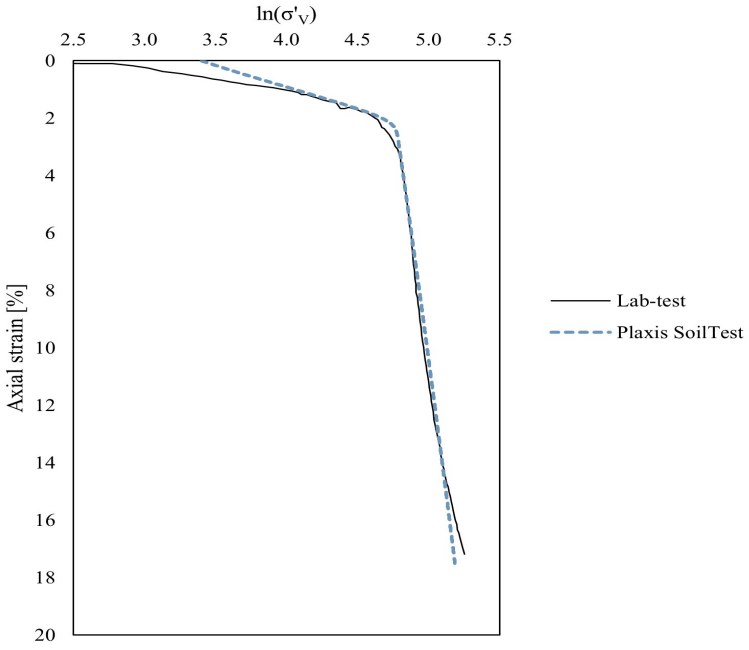

Figure A.5: Calibration of curves from Lab-test and Plaxis SoilTest at 18m depth, BH10010.

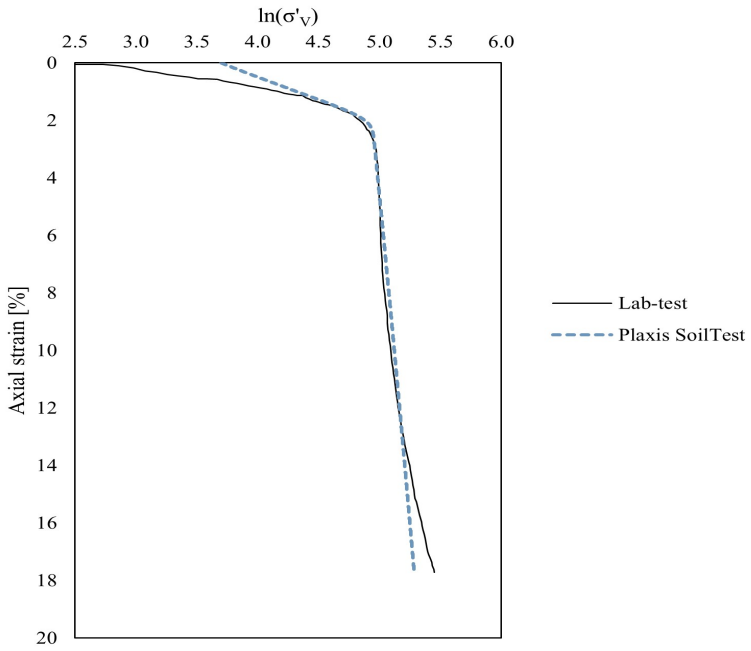

Figure A.6: Calibration of curves from Lab-test and Plaxis SoilTest at 21m depth, BH10010.

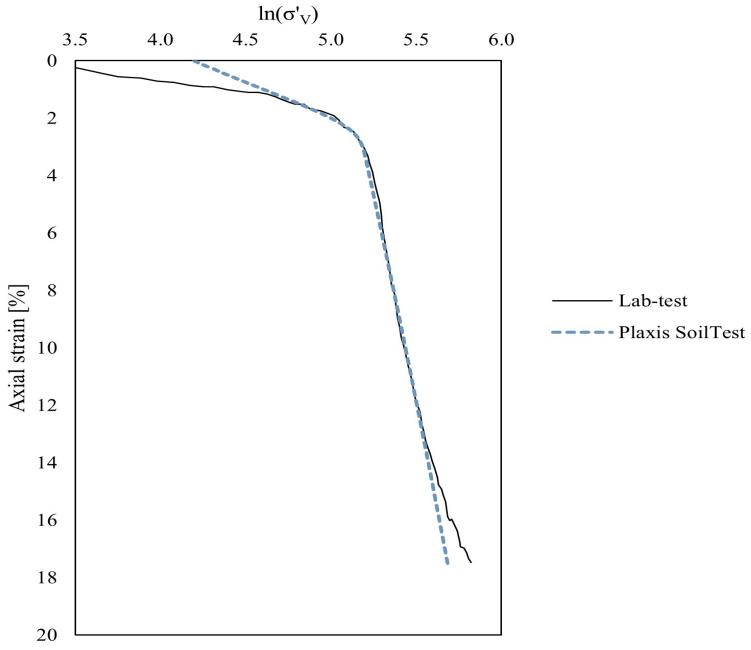

Figure A.7: Calibration of curves from Lab-test and Plaxis SoilTest at 27m depth, BH10010.

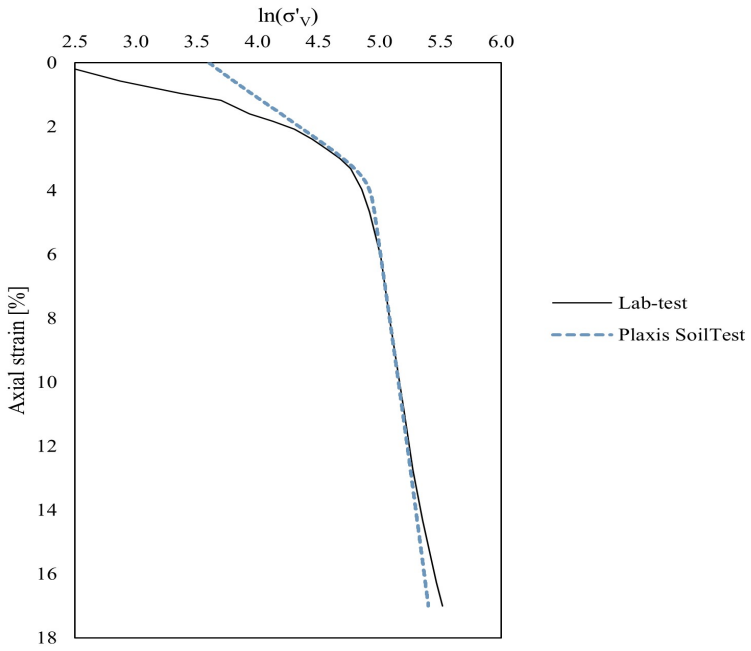

Figure A.8: Calibration of curves from Lab-test and Plaxis SoilTest at 24m depth, BH10010b.

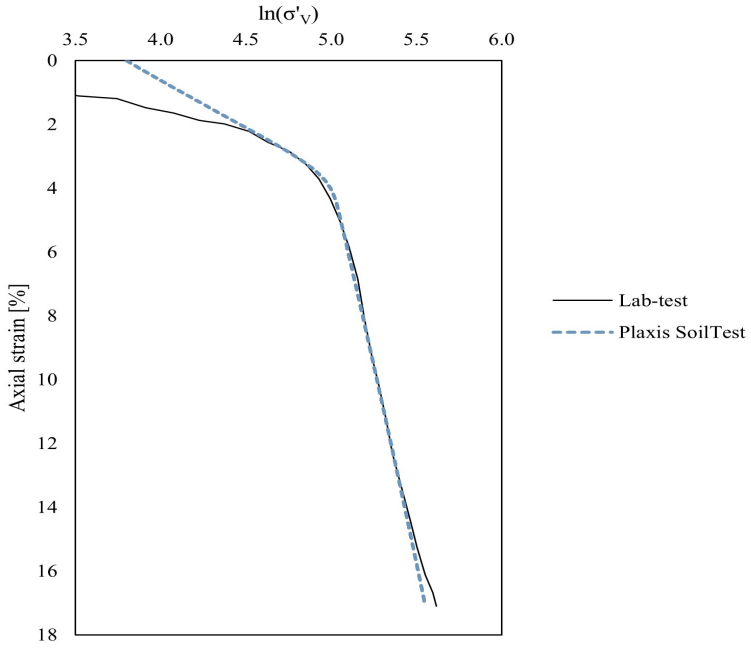

Figure A.9: Calibration of curves from Lab-test and Plaxis SoilTest at 26m depth, BH10010b.

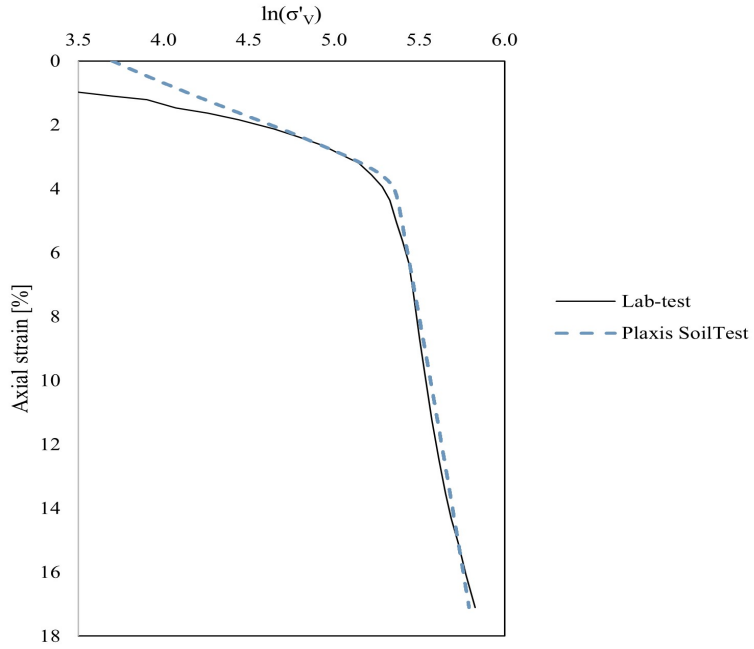

Figure A.10: Calibration of curves from Lab-test and Plaxis SoilTest at 30m depth, BH10010b.

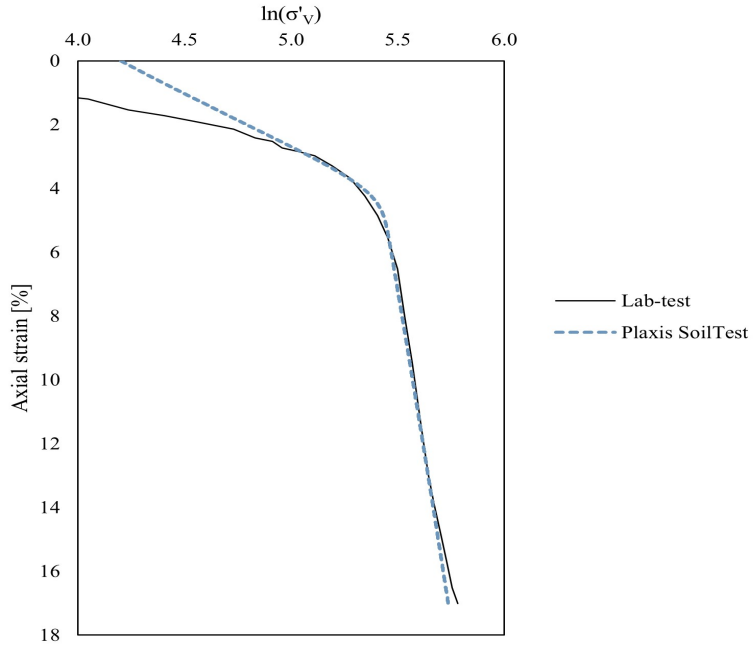

Figure A.11: Calibration of curves from Lab-test and Plaxis SoilTest at 32m depth, BH10010b.

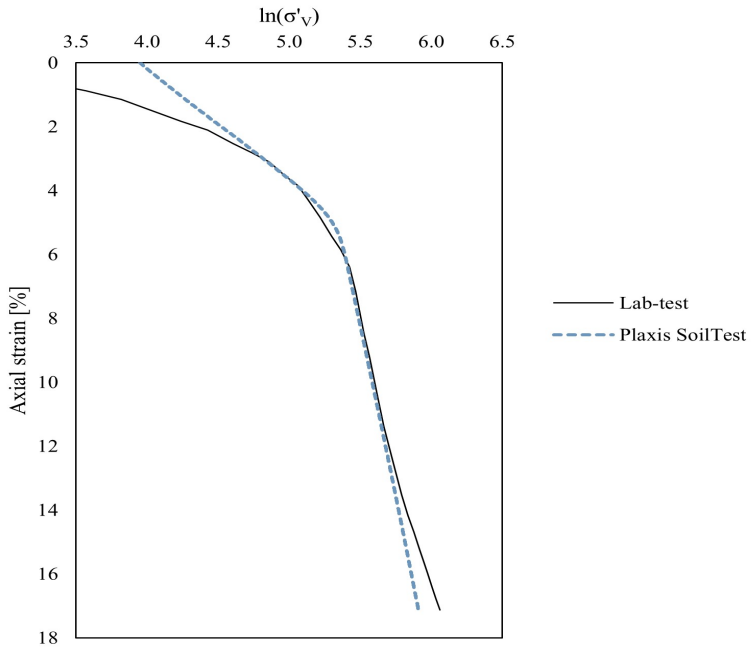

Figure A.12: Calibration of curves from Lab-test and Plaxis SoilTest at 34m depth, BH10010b.

B

Mesh Sensitivity Analysis

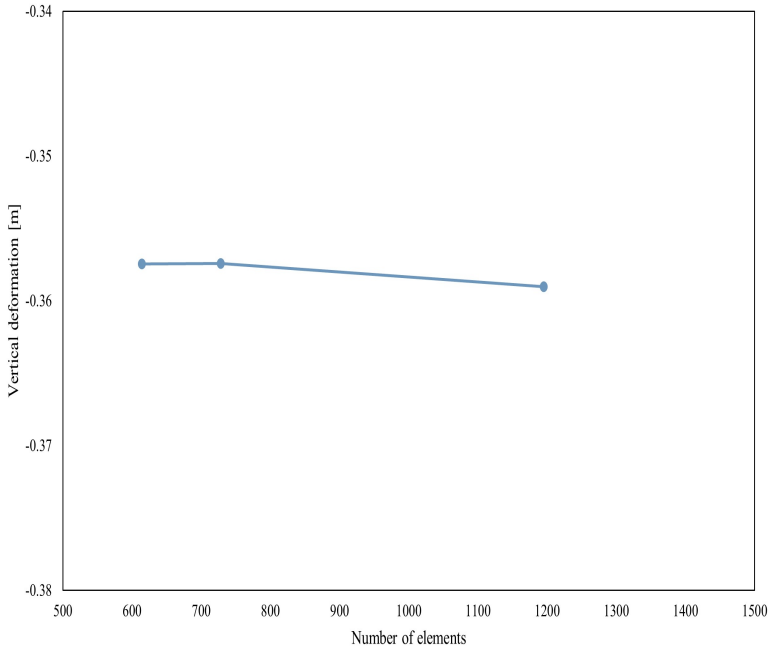

Figure B.1: Vertical deformation at 2 m depth for different number of elements.

Table B.1: Vertical deformation at 2 m depth for different number of elements.

Number of elements	Vertical deformation [m]
614	-0.357
728	-0.357
1195	-0.359

C

Modified Hydraulic Conductivity

Table C.1: Different hydraulic conductivities used for each model.

Analysis	**Hydraulic conductivity clay [m/day]**	**Hydraulic conductivity column [m/day]**	f_t **[kPa]**
Trafikverket Gx5 k1	$6.48 \cdot 10^{-5}$	$2.38 \cdot 10^{-3}$	8
Trafikverket Gx5 k2	$5.94 \cdot 10^{-5}$	$1.89 \cdot 10^{-3}$	10
Trafikverket Gx5 k3	$5 \cdot 10^{-5}$	$1 \cdot 10^{-3}$	11

D

Sensitivity Analysis

Table D.1: Values of swelling index for the sensitivity analysis.

Layer	Swelling index, κ low [-]	Swelling index, κ high [-]
Layer 1	0.047	0.067
Layer 2	0.047	0.067
Layer 3	0.04	0.06
Layer 4	0.04	0.06
Layer 5	0.05	0.07
Layer 6	0.055	0.075

Table D.2: Values of compression index for the sensitivity analysis.

Layer	Compression index, λ low [-]	Compression index, λ high [-]
Layer 1	0.9	1.1
Layer 2	0.9	1.1
Layer 3	0.95	1.15
Layer 4	0.87	1.07
Layer 5	0.8	1
Layer 6	0.8	1

Table D.3: Values of POP for the sensitivity analysis.

Layer	POP low [kPa]	POP high [kPa]
Layer 1	3	13
Layer 2	9	19
Layer 3	14	24
Layer 4	15	25
Layer 5	22	32
Layer 6	35	45

Table D.4: Values of μ for the different κ and λ used in the sensitivity analysis.

Layer	μ **for** κ **low [-]**	μ **for** κ **high [-]**	μ **for** λ **low [-]**	μ **for** λ **high [-]**
Layer 1	2.05	2.10	2.32	1.88
Layer 2	2.05	2.10	2.32	1.88
Layer 3	1.94	1.98	2.17	1.78
Layer 4	2.10	2.15	2.39	1.92
Layer 5	2.30	2.36	2.64	2.08
Layer 6	2.31	2.37	2.66	2.09

E

Stress-Strain Curves

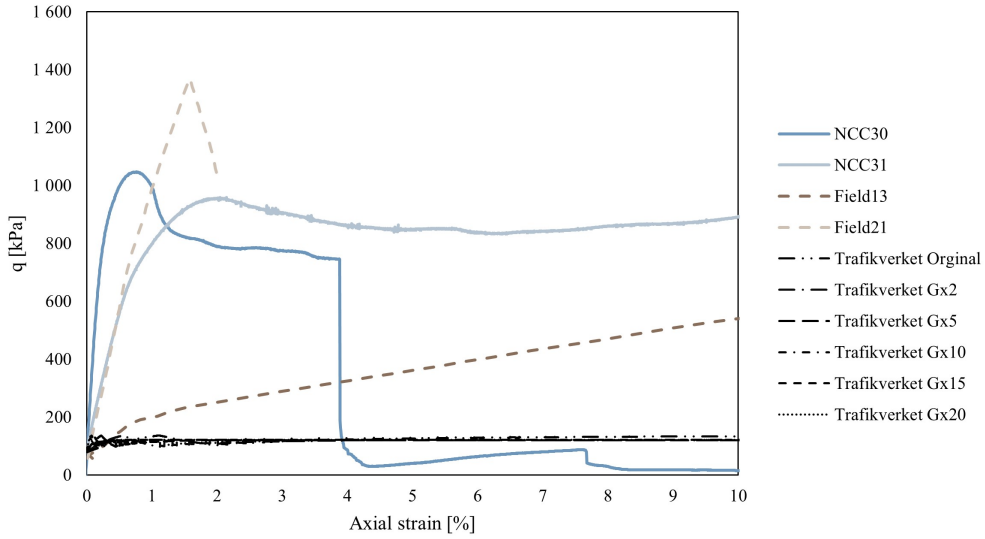

Figure E.1: Stress-Strain curves from laboratory and Plaxis 2D analyses.

DEPARTMENT OF ARCHITECTURE AND CIVIL ENGINEERING
CHALMERS UNIVERSITY OF TECHNOLOGY
Gothenburg, Sweden
www.chalmers.se

CHALMERS
UNIVERSITY OF TECHNOLOGY